Detectors at HL-LHC and Future Colliders

55th International Winter Meeting on Nuclear Physics

W. Riegler, CERN

Particle Detector

A particle detector is a device, that is collapsing wavefunctions of quantum mechanical states, which themselves are linear superpositions of irreducible representations of the inhomogeneous Lorentz Group.

Particle Detector

A particle is an irreducible representation of the inhomogeneous Lorentz group.

ON UNITARY REPRESENTATIONS OF THE INHOMOGENEOUS LORENTZ GROUP*

By E. WIGNER

(Received December 22, 1937)

of the invariance of the transition probability we have

(1) $$|(\varphi_l, \psi_l)|^2 = |(\varphi_{l'}, \psi_{l'})|^2$$

and it can be shown[4] that the aforementioned constants in the $\varphi_{l'}$ can be chosen in such a way that the $\varphi_{l'}$ are obtained from the φ_l by a linear unitary operation, depending, of course, on l and l'

(2) $$\varphi_{l'} = D(l', l)\varphi_l .$$

By going over from a first system of reference l to a second $l' = L_1 l$ and then to a third $l'' = L_2 L_1 l$ or directly to the third $l'' = (L_2 L_1) l$, one must obtain—apart from the above mentioned constant—the same set of wave functions. Hence from

$$\varphi_{l''} = D(l'', l')D(l', l)\varphi_l$$

$$\varphi_{l''} = D(l'', l)\varphi_l$$

it follows

(3) $$D(l'', l')D(l', l) = \omega D(l'', l)$$

D. Classification of unitary representations from the point of view of infinitesimal operators

→ Scalars, spinors, vectors

→ m>0 and s=0, 1/2, 1, 3/2, 2

Particle Detector

Wilson Cloud Chamber 1911

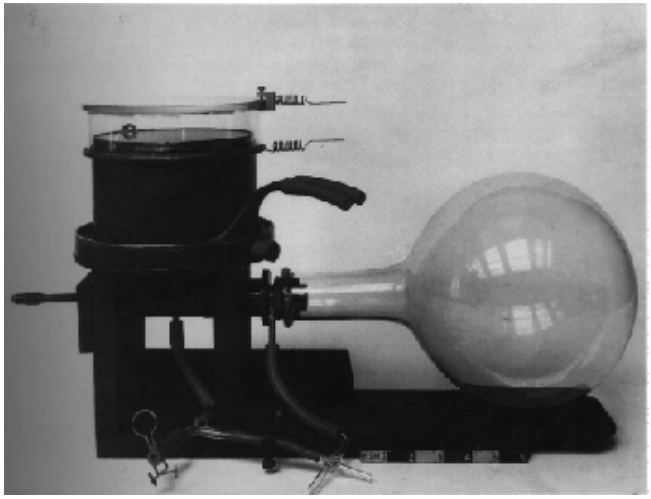

Wilson's cloud chamber played a key role in particle physics from it's invention in 1911 to the 1950ies, and it also played an important role in the discussion of the interactions of 'quantum systems' with 'classical measurement devices'

Early Alpha-Ray picture, Wilson 1912

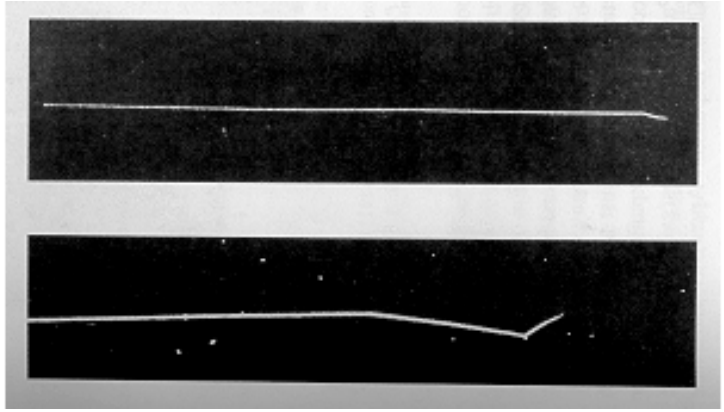

Alphas, Philipp 1926

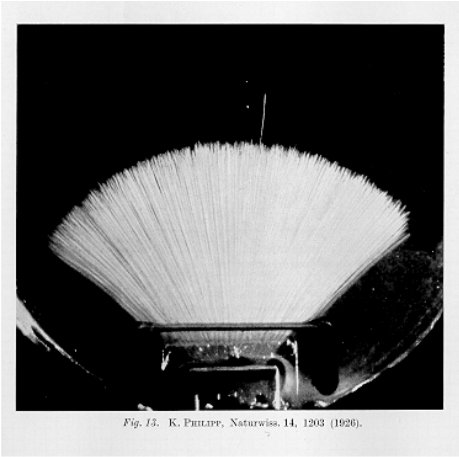

Fig. 13. K. Philipp, Naturwiss. 14, 1203 (1926).

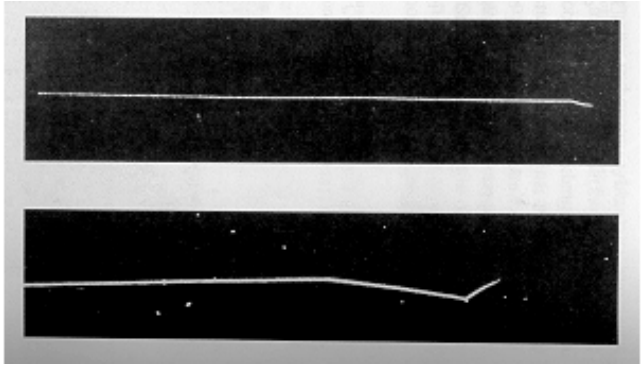

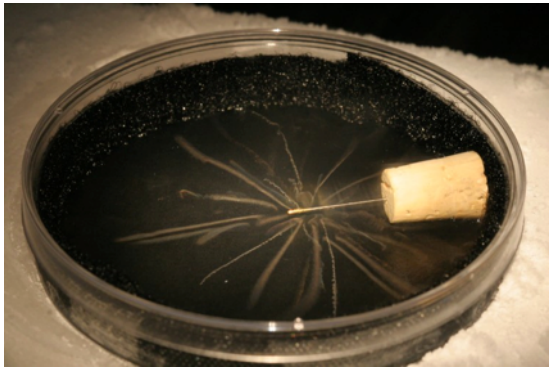

Solvay Conference 1927, Einstein:
"A radioactive sample emits alpha particles in all directions; these are made visible by the method of the Wilson Cloud Chamber. Now, if one associates a spherical wave with each emission process, how can one understand that the track of each alpha particle appears as a (very nearly) straight line …. "

Born, Heisenberg:
"As soon as such an ionization is shown by the appearance of cloud droplets, in order to describe what happens afterwards one must reduce the wave packet in the immediate vicinity of the drops. One thus obtains a wave packet in the form of a ray, which corresponds to the corpuscular character of the phenomenon."

According to this reasoning the whole process is described in terms of the interaction of a quantum system (the alpha particle) with a classical measurement apparatus (the atoms of the vapour).

Nevill Mott (1929):
Assuming the atoms of the vapour also to be part of the quantum mechanical system, " … it is a little difficult to picture how it is that an outgoing spherical wave can produce a straight track; we think intuitively that it should ionise atoms at random throughout space."

Mott considers and example with and alpha particle at the origin, one hydrogen atom at position $\mathbf{a}_1$ and another hydrogen atom at $\mathbf{a}_2$, and the two hydrogen atoms only having EM interaction with the alpha particle:

[Mo] Mott N.F., The wave mechanics of α-ray tracks. *Proc. R. Soc. Lond. A*, **126**, 79-84, 1929. Reprinted in: Wheeler J.A., Zurek W., *Quantum Theory and Measurement*, Princeton University Press, 1983.

Main objects of the investigation are periodic solutions $F(\boldsymbol{R}, \boldsymbol{r_1}, \boldsymbol{r_2})e^{iEt/\hbar}$ of the Schrödinger equation for the three particle system, where $\boldsymbol{R}$, $\boldsymbol{r_1}$, $\boldsymbol{r_2}$ denote the coordinates of the α-particle and of the two hydrogen atom electrons respectively. The function F (depending parametrically on E) is solution of the stationary Schrödinger equation

$$-\frac{\hbar^2}{2M}\Delta_R F + \Big(-\frac{\hbar^2}{2m}\Delta_{r_1} - \frac{e^2}{|\boldsymbol{r_1}-\boldsymbol{a_1}|}\Big)F + \Big(-\frac{\hbar^2}{2m}\Delta_{r_2} - \frac{e^2}{|\boldsymbol{r_2}-\boldsymbol{a_2}|}\Big)F$$
$$-\Big(\frac{2e^2}{|\boldsymbol{R}-\boldsymbol{r_1}|} + \frac{2e^2}{|\boldsymbol{R}-\boldsymbol{r_2}|}\Big)F = E\,F \qquad (4.1)$$

where Δ_x is the laplacian with respect to the coordinate x, M is the mass of the α-particle, m is the mass of the electron, $-e$ is the charge of the electron so that $2e$ is the charge of the α-particle.

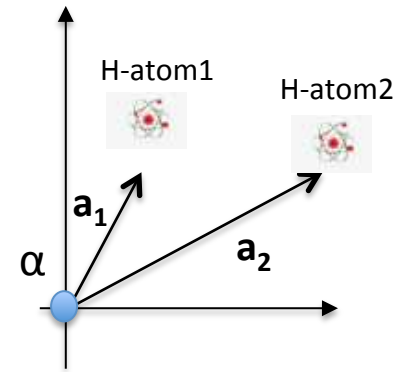

Result: The two hydrogen atoms cannot both be excited (or ionized) unless $\mathbf{a}_1$, $\mathbf{a}_1$ and the origin lie on the same straight line.
(see Also Werner Heisenberg, Chicago lectures 1930)

This example (i.e. moving the boundary between the quantum system and classical measurements device) is also used by S. Coleman in the lecture
Quantum Mechanics in Your Face [1994] https://www.youtube.com/watch?v=EtyNMlXN-sw
to show how the collapse of the wave function and other 'interpretations of QM' become unnecessary if one removes this boundary and simply considers the entire world (including us) as QM systems.

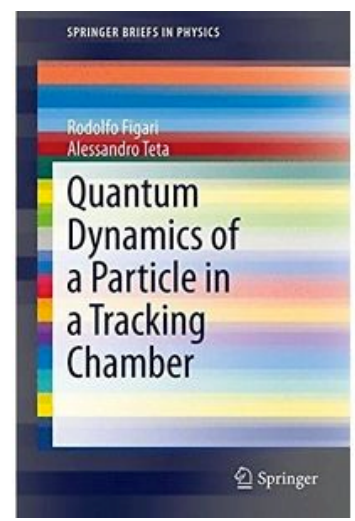

Renninger's negative-result experiment (1953)

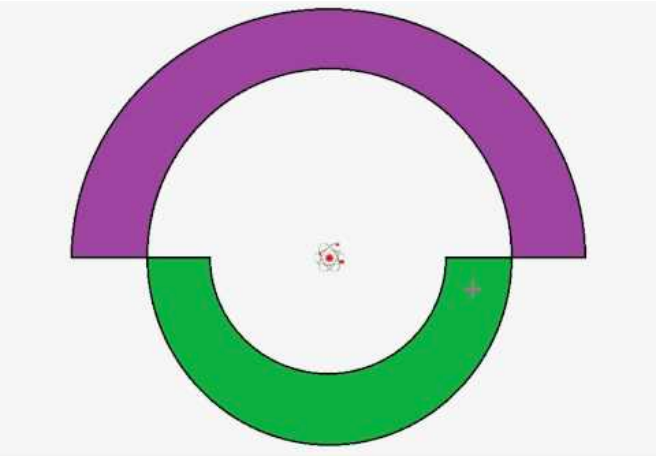

A radioactive atom (emitting and alpha particle) is placed in the center of a detector that consists of two hemispheres and that are 100% efficient to alpha particles.

Considering the second (purple) hemisphere to be very large, the absence of the a signal on the green detector after a given time will indicate that the alpha particle will hit the purple detector.

The QM analysis will come out right, with a given probability for the red or the green part to fire and zero probability that both fire.

The semi-classical analysis is however confusing:
The wavefunction has collapsed although there was no measurement performed with the green detector ?
A non measurement collapses a wavefunction ?

CERN Circular Colliders and FCC

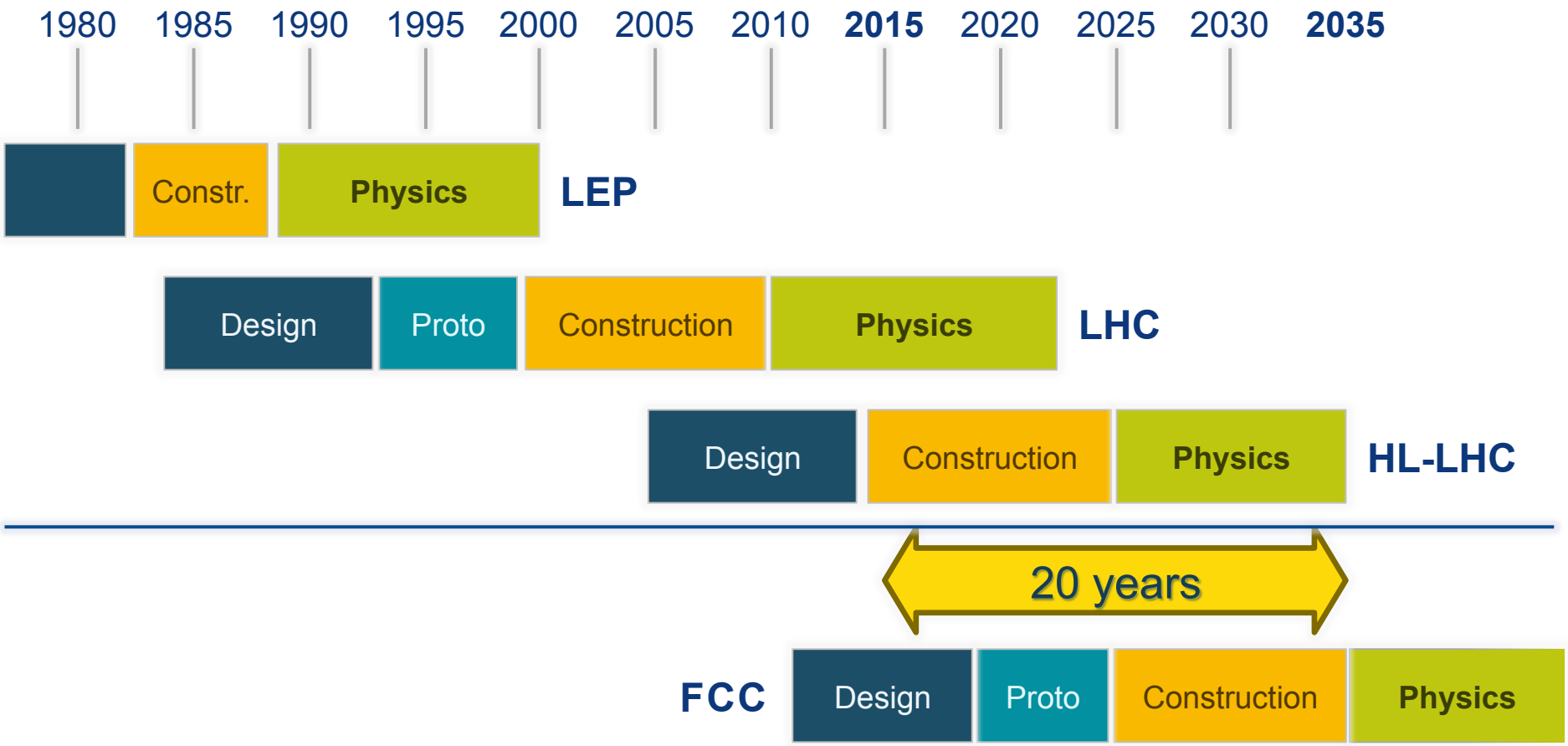

FCC Conceptual Design Report by end 2018 for the European strategy update

Future Circular Collider Study

International FCC collaboration (CERN as host lab) to study:

- ***pp*-collider (*FCC-hh*)**
  → main emphasis, defining infrastructure requirements

~16 T ⇒ 100 TeV *pp* in 100 km

- **80-100 km infrastructure** in Geneva area
- **e^+e^- collider (*FCC-ee*)** as potential intermediate step
- ***p-e* (FCC-he) option**
- **HE-LHC** with FCC-hh technology

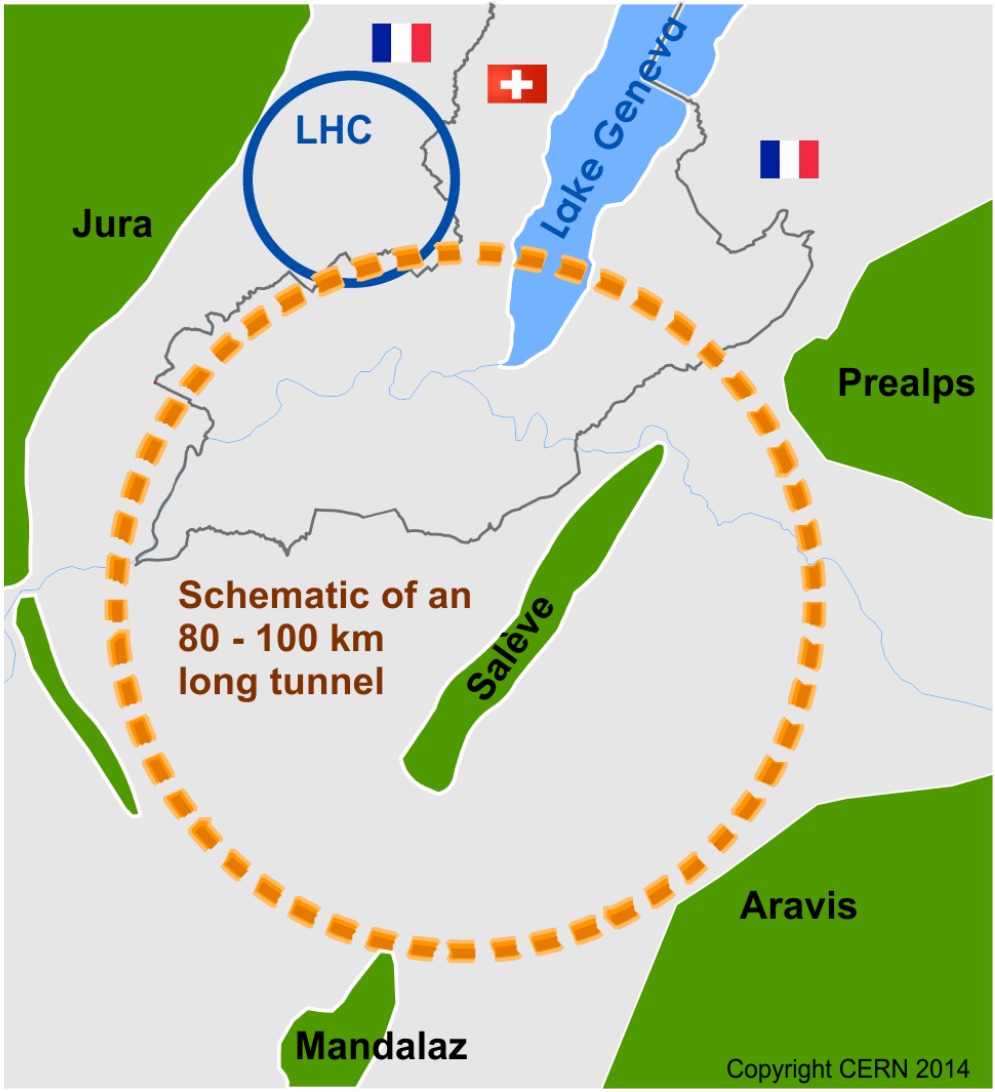

FCC-hh as a Heavy Ion Collider

Heavy ions at the Future Circular Collider

https://arxiv.org/pdf/1605.01389v3.pdf

A. Dainese [1], *U.A. Wiedemann* [2] *(editors), N. Armesto* [3], *D. d'Enterria* [2], *J.M. Jowett* [2], *J.-P. Lansberg* [4], *J.G. Milhano* [5,2], *C.A. Salgado* [3], *M. Schaumann* [2], *M. van Leeuwen* [6,7] *(section editors), J.L. Albacete* [8], *A. Andronic* [9], *P. Antonioli* [10], *L. Apolinário* [5], *S. Bass* [11], *A. Beraudo* [12], *A. Bilandzic* [13], *S. Borsanyi* [14], *P. Braun-Munzinger* [9], *Z. Chen* [15], *L. Cunqueiro Mendez* [16], *G.S. Denicol* [17], *K.J. Eskola* [18], *S. Floerchinger* [19], *H. Fujii* [20], *P. Giubellino* [12], *C. Greiner* [21], *J.F. Grosse-Oetringhaus* [2], *C.-M. Ko* [22], *P. Kotko* [23], *K. Krajczár* [2,24], *K. Kutak* [25], *M. Laine* [26], *Y. Liu* [27], *M.P. Lombardo* [28], *M. Luzum* [29,3], *C. Marquet* [30], *S. Masciocchi* [9], *V. Okorokov* [31], *J.-F. Paquet* [32,33], *H. Paukkunen* [3,18,34], *E. Petreska* [30,3], *T. Pierog* [35], *M. Ploskon* [36], *C. Ratti* [37], *A.H. Rezaeian* [38], *W. Riegler* [2], *J. Rojo* [39], *C. Roland* [24], *A. Rossi* [40,1], *G.P. Salam* [2], *S. Sapeta* [25,2], *R. Schicker* [19], *C. Schmidt* [41], *J. Stachel* [19], *J. Uphoff* [21], *A. van Hameren* [25], *K. Watanabe* [42], *B.-W. Xiao* [42], *F. Yuan* [36], *D. Zaslavsky* [42], *K. Zhou* [21,15], *P. Zhuang* [15]

Abstract

The Future Circular Collider (FCC) Study is aimed at assessing the physics potential and the technical feasibility of a new collider with centre-of-mass energies, in the hadron–hadron collision mode, seven times larger than the nominal LHC energies. Operating such machine with heavy ions is an option that is being considered in the accelerator design studies. It would provide, for example, Pb–Pb and p–Pb collisions at $\sqrt{s_{\mathrm{NN}}} = 39$ and 63 TeV, respectively, per nucleon–nucleon collision, with integrated luminosities above 30 nb^{-1} per month for Pb–Pb. This is a report by the working group on heavy-ion physics of the FCC Study. First ideas on the physics opportunities with heavy ions at the FCC are presented, covering the physics of the Quark–Gluon Plasma, of gluon saturation, of photon-induced collisions, as well as connections with other fields of high-energy physics.

FCC-hh as heavy ion collider shows interesting luminosity evolution along the fill:

Beam and Luminosity Evolution

During the beams are in collision the instantaneous value of the luminosity will change:

$$\mathcal{L}(t) = A \frac{N_b^2(t)}{\sqrt{\epsilon_x(t)\epsilon_y(t)}}$$

The beam evolution with time is obtained by solving a system of four differential equations (dominant effects only shown here, more included in simulations):

$$\frac{\mathrm{d}N_b}{\mathrm{d}t} = -\sigma_{c,\mathrm{tot}} A \frac{N_b^2}{\sqrt{\epsilon_x \epsilon_y}}$$

Intensity

$$\frac{\mathrm{d}\epsilon_x}{\mathrm{d}t} = \epsilon_x(\alpha_{\mathrm{IBS},x} - \alpha_{\mathrm{rad},x})$$

Hor. Emittance

$$\frac{\mathrm{d}\epsilon_y}{\mathrm{d}t} = \epsilon_y(\alpha_{\mathrm{IBS},y} - \alpha_{\mathrm{rad},y})$$

Ver. Emittance

$$\frac{\mathrm{d}\sigma_s}{\mathrm{d}t} = \frac{1}{2}\sigma_s(\alpha_{\mathrm{IBS},s} - \alpha_{\mathrm{rad},s})$$

Bunch Length

with

$$A = f_{\mathrm{rev}} k_b / (4\pi\beta^*)$$

f_{rev} : revolution freq.
k_b : no. bunches/beam
β^* : β-function at IP
N_b : no. particles/bunch
ϵ : geom. emittances
σ_s : bunch length

$\sigma_{c,\mathrm{tot}}$: total cross-section
α_{IBS} : IBS growth rate
α_{rad} : rad. damping rate

J. Jowett, M. Schaumann, FCC week Washington 2015

Effects on the Emittance – a new regime

Intra-Beam Scattering (IBS)

Multiple small-angle Coulomb scattering within a charged particle beam.

Emittance Growth

Growth rate dynamically changing with **beam properties**:

$$\alpha_{IBS} \propto \frac{r_0^2}{\gamma^4} \boxed{\frac{N_b}{\epsilon_x \epsilon_y \sigma_s \sigma_p}}$$

IBS is weak for initial beam parameters, but increases with decreasing emittance .

Growth Times	Unit	FCC @ 50Z TeV
	[h]	29.1
	[h]	30.0

(Synchrotron) Radiation Damping

A charged particle radiates energy, when it is accelerated, i.e. bend on its circular orbit.

Emittance Shrinkage

Damping rate is **constant** for a given energy:

$$\alpha_{rad} \propto \frac{E^3 C_\alpha}{\rho_0 C_{ring}}$$

$$\frac{\alpha_{\mathrm{rad,FCC}}}{\alpha_{\mathrm{rad,LHC}}} \approx \frac{E^3_{\mathrm{FCC}}/C^2_{\mathrm{FCC}}}{E^3_{\mathrm{LHC}}/C^2_{\mathrm{LHC}}} \approx \frac{7^3}{4^2} \approx 22$$

Damping Times	Unit	FCC @ 50Z TeV
	[h]	0.24
	[h]	0.49

Fast emittance decrease at the beginning of the fill, until IBS becomes strong enough to counteract the radiation damping.

Pb-Pb Luminosity Evolution

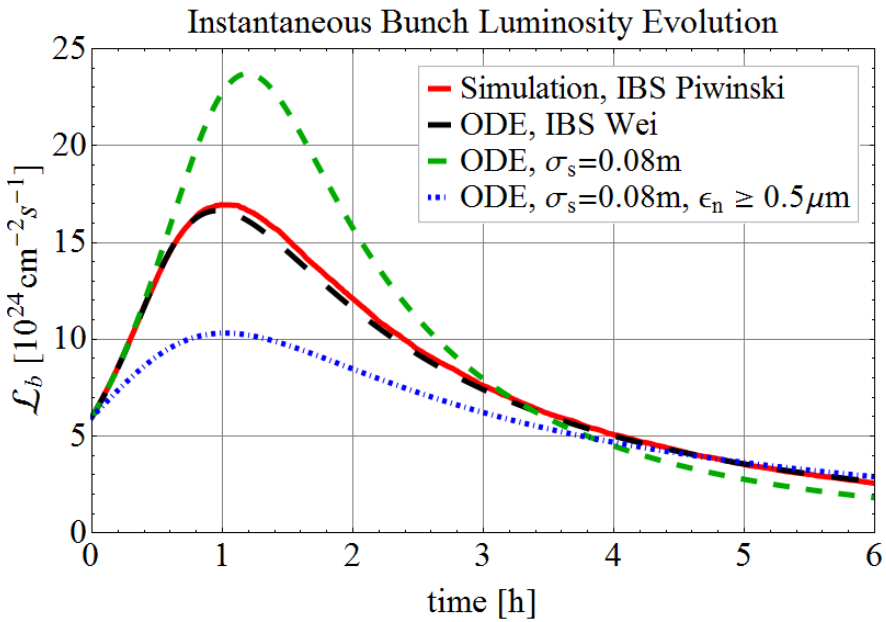

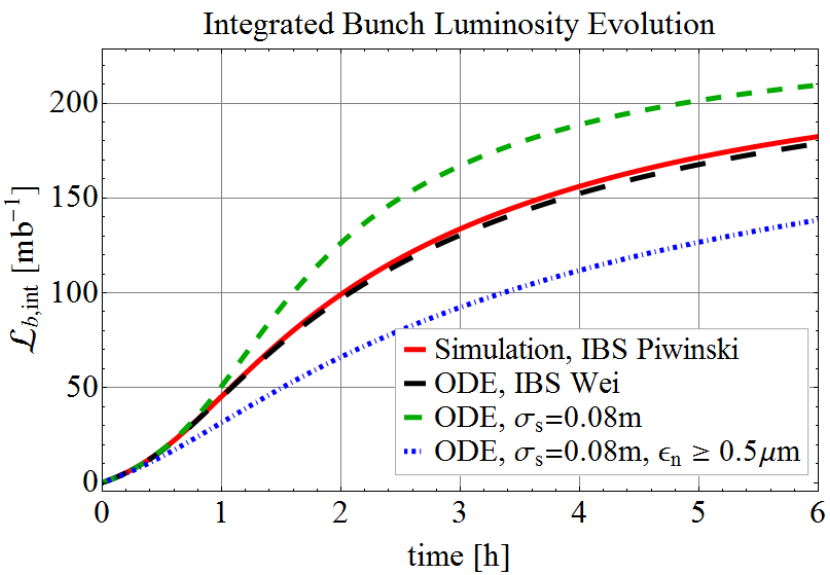

FCC-hh general purpose detector: Twin Solenoid + Dipole Magnet System

Matthias Mentink, Alexey Dudarev, Helder Filipe Pais Da Silva, Christophe Paul Berriaud, Gabriella Rolando, Rosalinde Pots, Benoit Cure, Andrea Gaddi, Vyacheslav Klyukhin, Hubert Gerwig, Udo Wagner, and Herman ten Kate

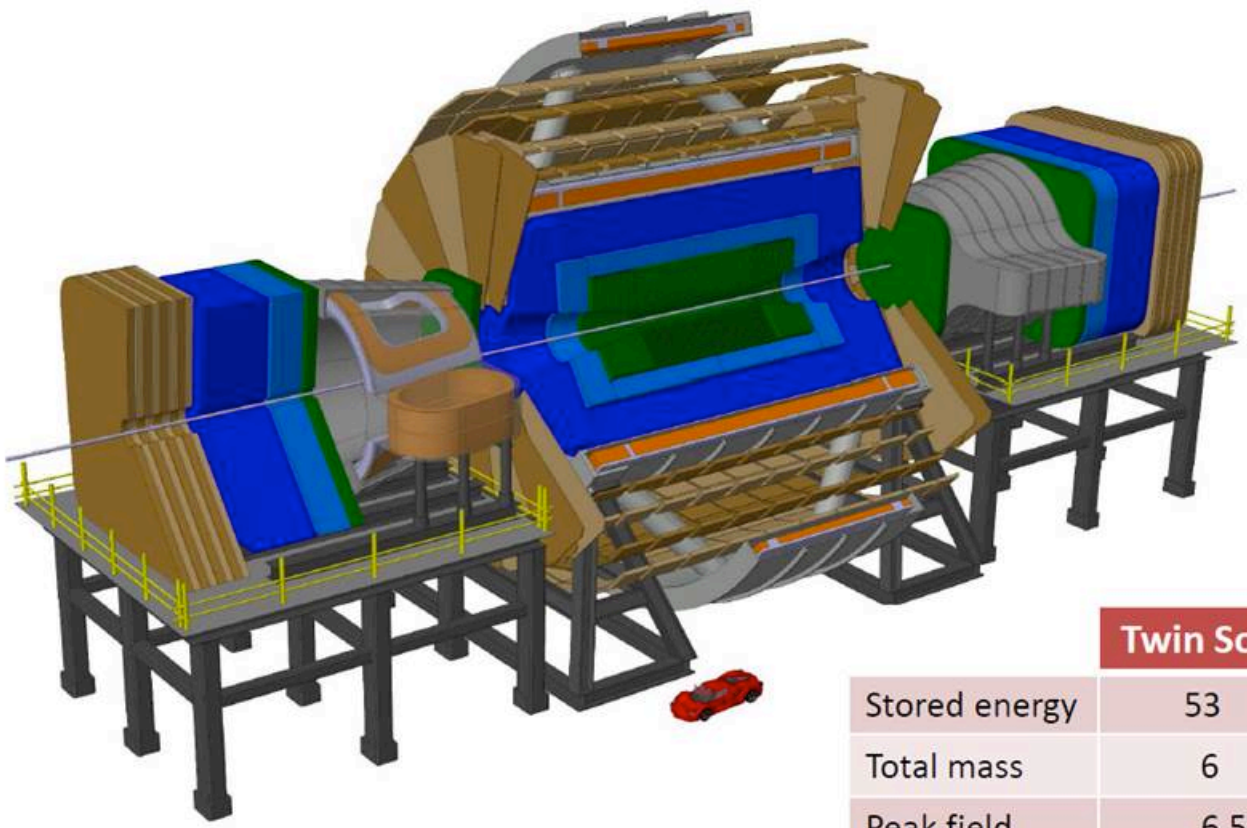

FCC Air core Twin solenoid and Dipoles

State of the art high stress / low mass design.

	Twin Solenoid	Dipole
Stored energy	53 GJ	2 x 1.5 GJ
Total mass	6 kt	0.5 kt
Peak field	6.5 T	6.0 T
Current	80 kA	20 kA
Conductor	102 km	2 x 37 km
Bore x Length	12 m x 20 m	6 m x 6 m

FCC-hh general purpose reference detector

100TeV pp collisions, $L_{peak} = 3x10^{35}\ cm^{-2}s^{-1}$, $L_{int} = 3/30\ ab^{-1}$
25ns/5ns bunchcrossing, pileup 1000/200 per bunchcrossing

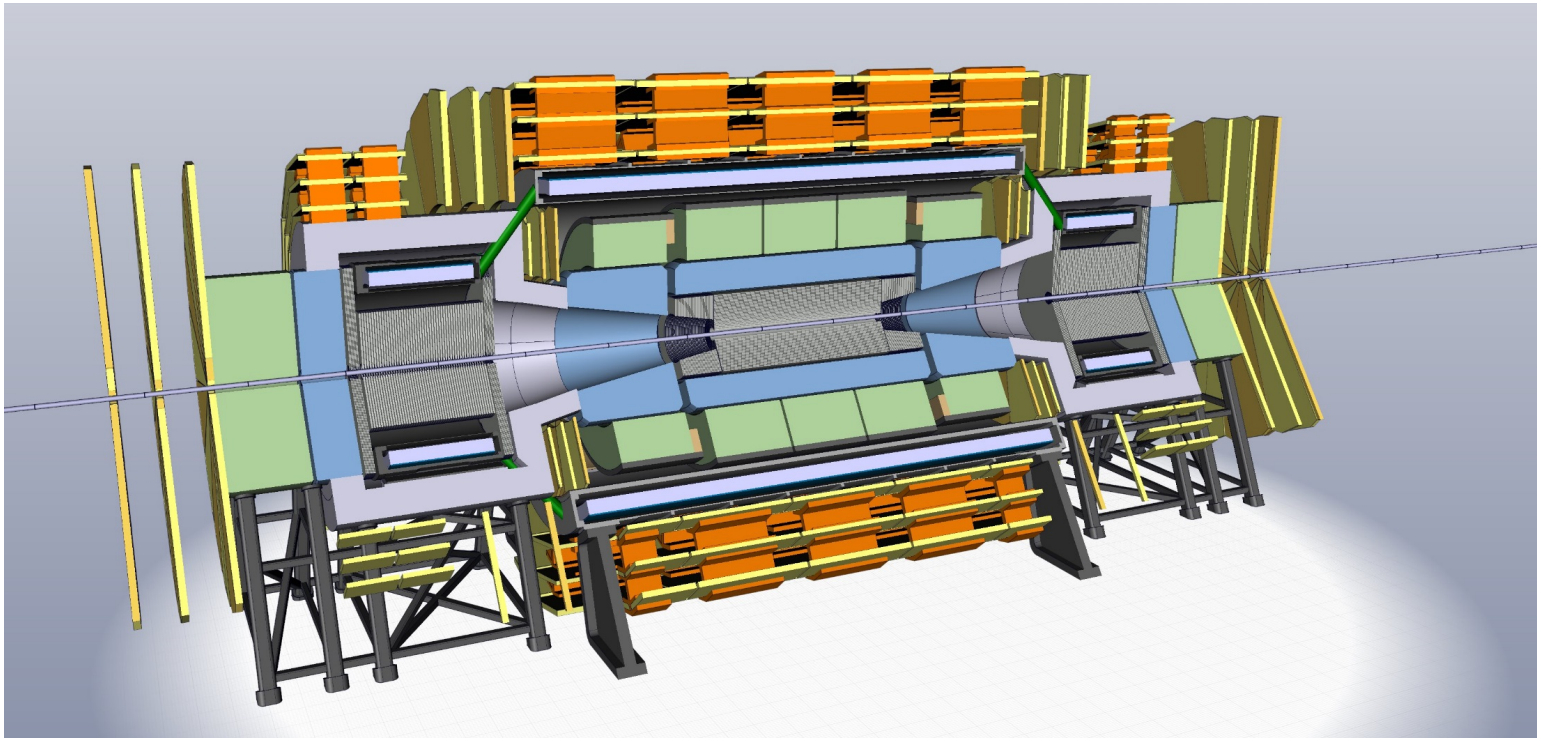

4T, 10m free bore unshielded solenoid, two 4T unshielded forward solenoids, precision spectroscopy and ECAL up to eta=4, Tracking and Calo up to eta=6

Radiation Calculations

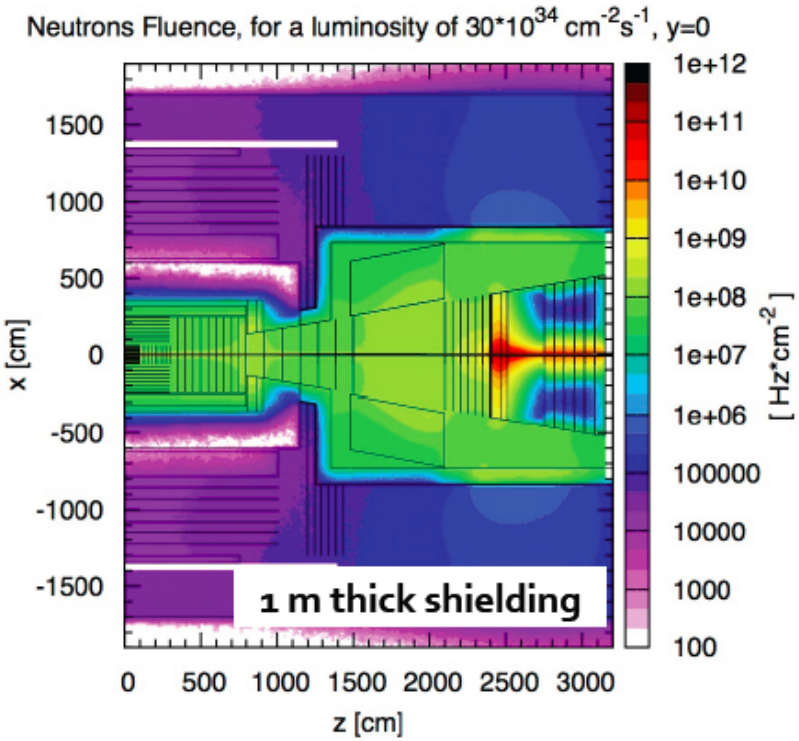

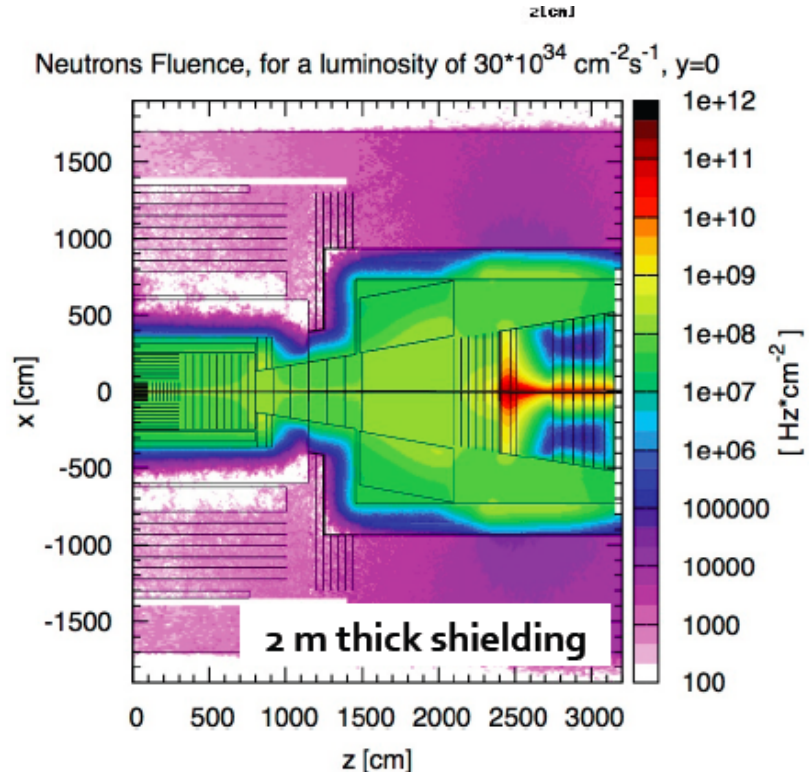

In the central tracker, close to the beampipe, the radiation is dominated by the primary hadrons.

In the forward tracker there is in addition a significant neutron flux from the calorimeter.

Radiation Calculations

1 MeV neutron equivalent fluence vs R at different z positions **in the tracker:**

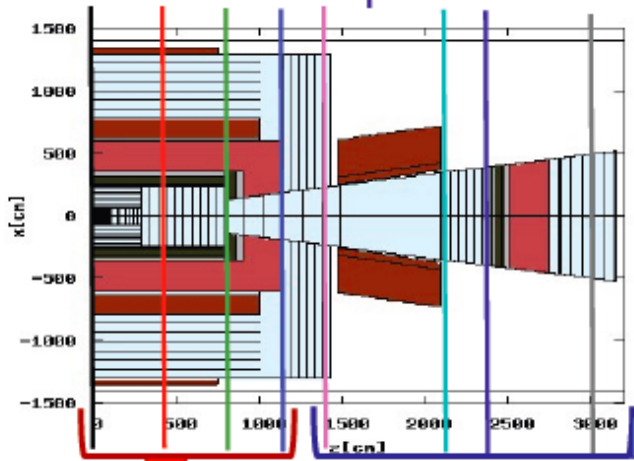

Forward region

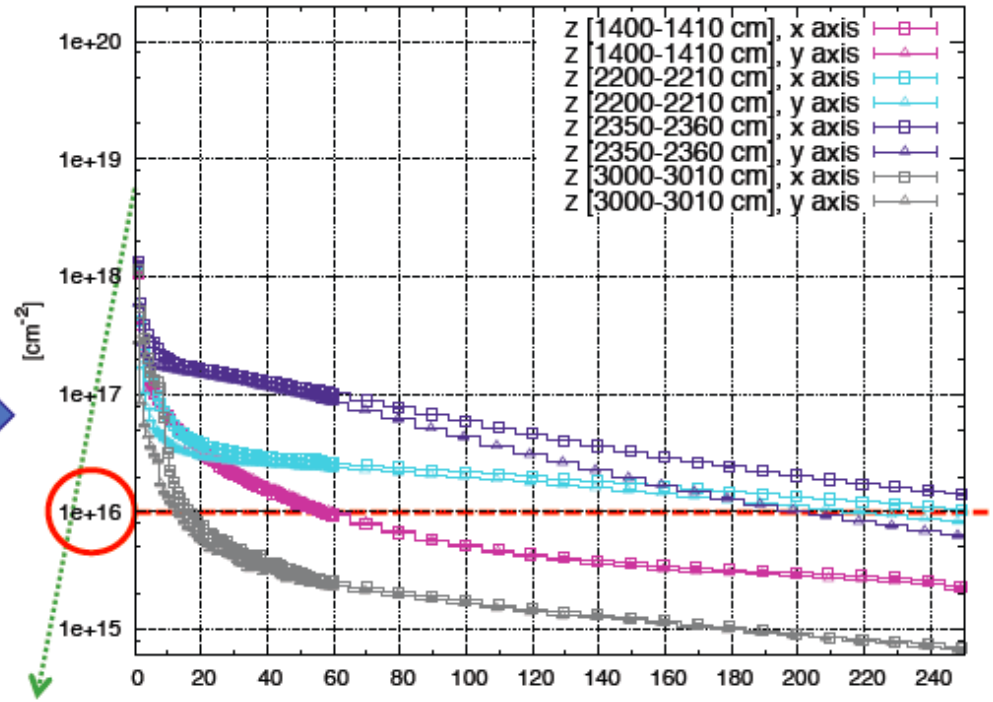

Central region

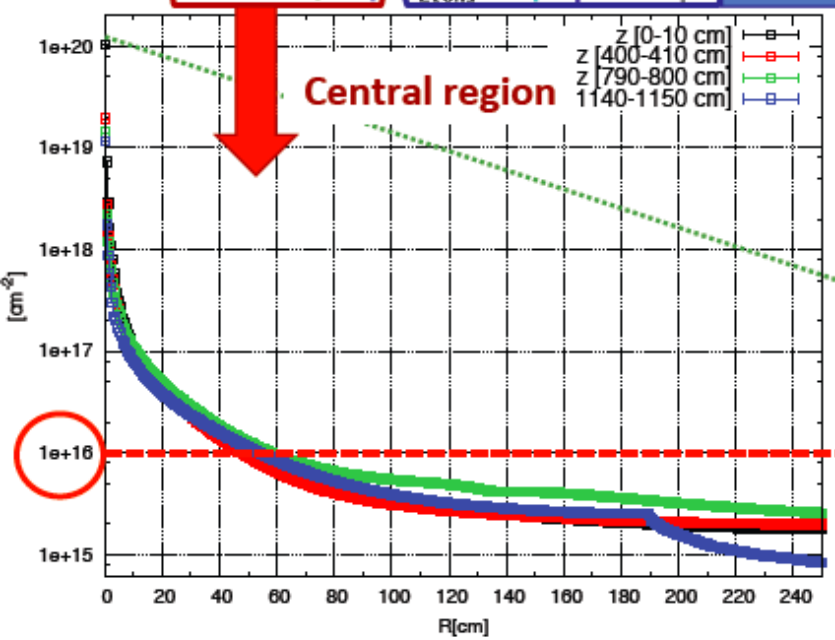

Different radial resolution!

For radii < 50 cm the fluence exceed the value expected at HL-LHC (10^{16} cm^{-2}) by up to 2 orders of magnitude → **Technology challenge!**

Fluence is even higher close to forward calorimeter: at z= 23.5 m the fluence vs x > 10^{16} cm^{-2} for x<2.5 m

Ilaria Besana

Detectors for Astronomy and Particle Physics

Newton Reflector 1668

Rutherford and Geiger 1908 'Geiger Counter'

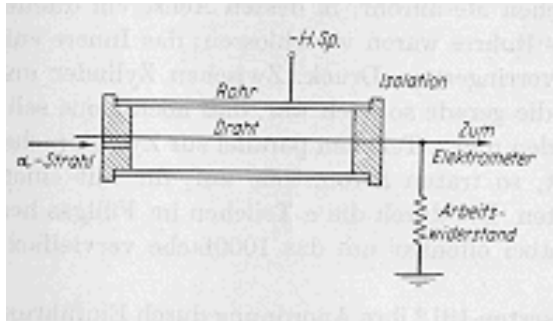

Cosmic ray telescope 1934

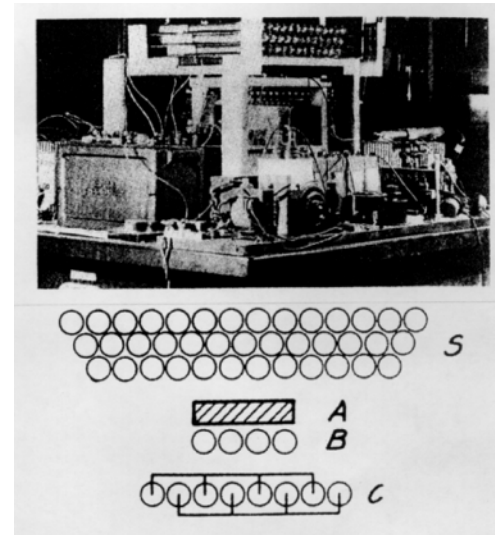

Very old 'principles' and even specific devices were enormously boosted in their performance by new readout technologies.

Telescopes:
Visual → photo → CCD → …

Detectors:
Photos → counting → microelectronics, computing

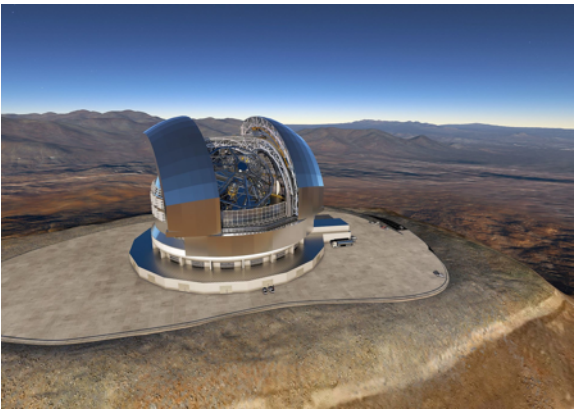

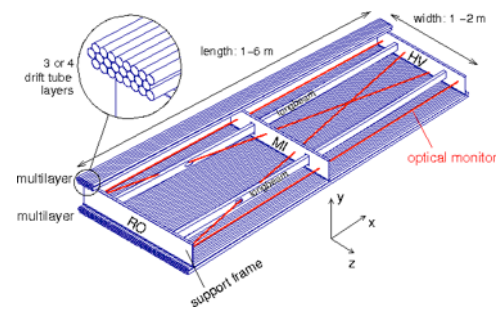

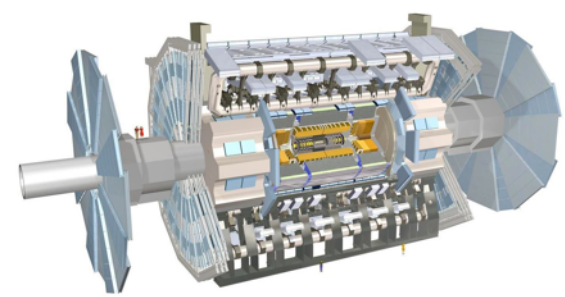

Future Triggering

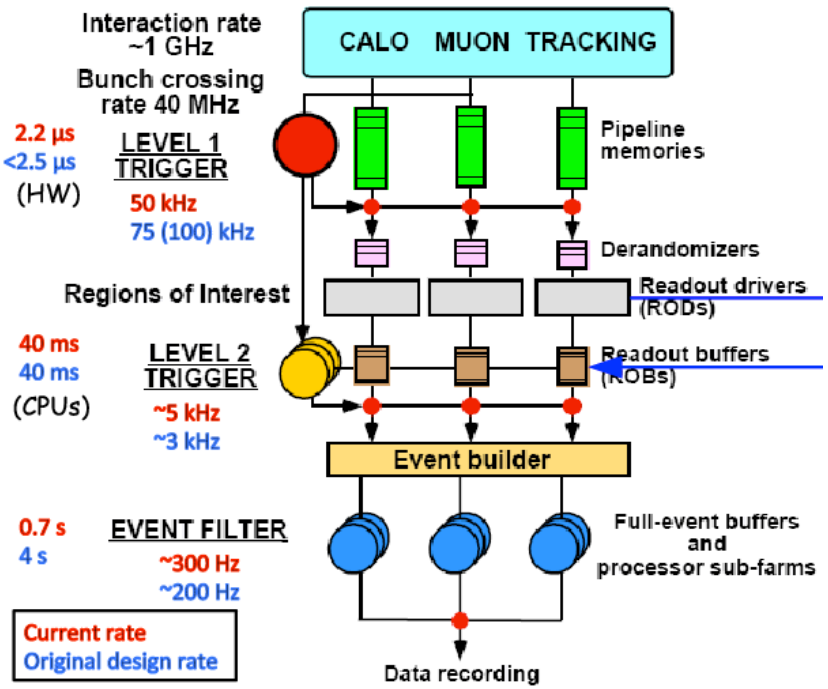

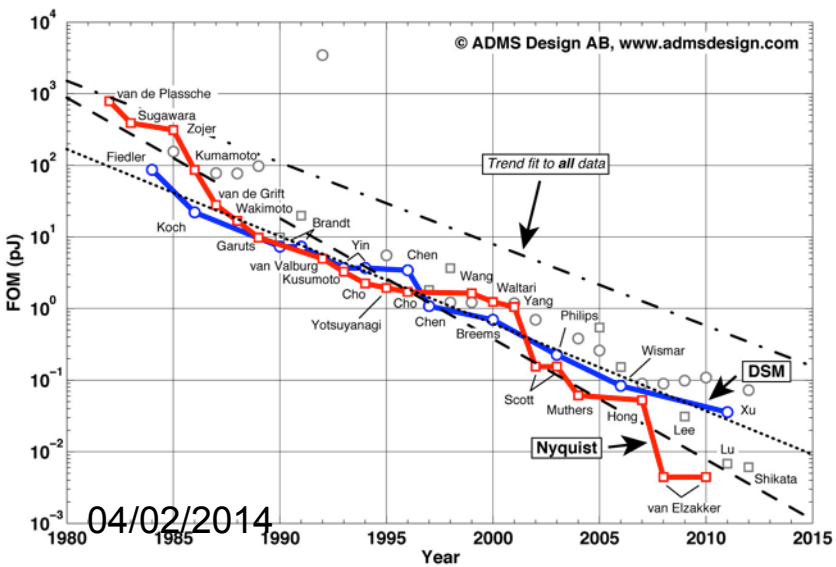

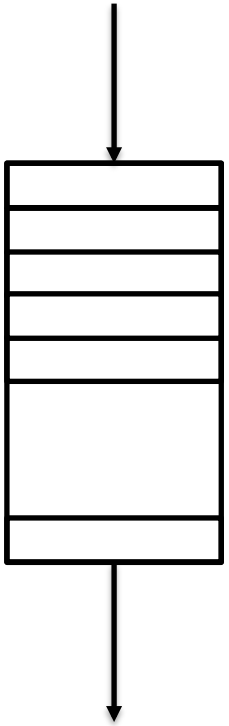

Pipeline Memories, e.g. ATLAS Liquid Argon Calorimeter:

Analog pipeline i.e. Switch Capacitor Array (SCA)

Up to now, full Digitization was not possible at 40MHz 12bit in 2005 due to excessive power consumption.

The power consumption of ADCs has however desreased dramatically over the last years i.e. for the LHC experiment upgrades, 40MHz digitization will be possible !

Data transferred to USA15 at 25TB/s.

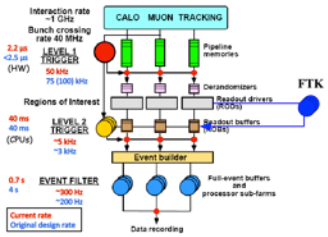

LHC to HL-HLC

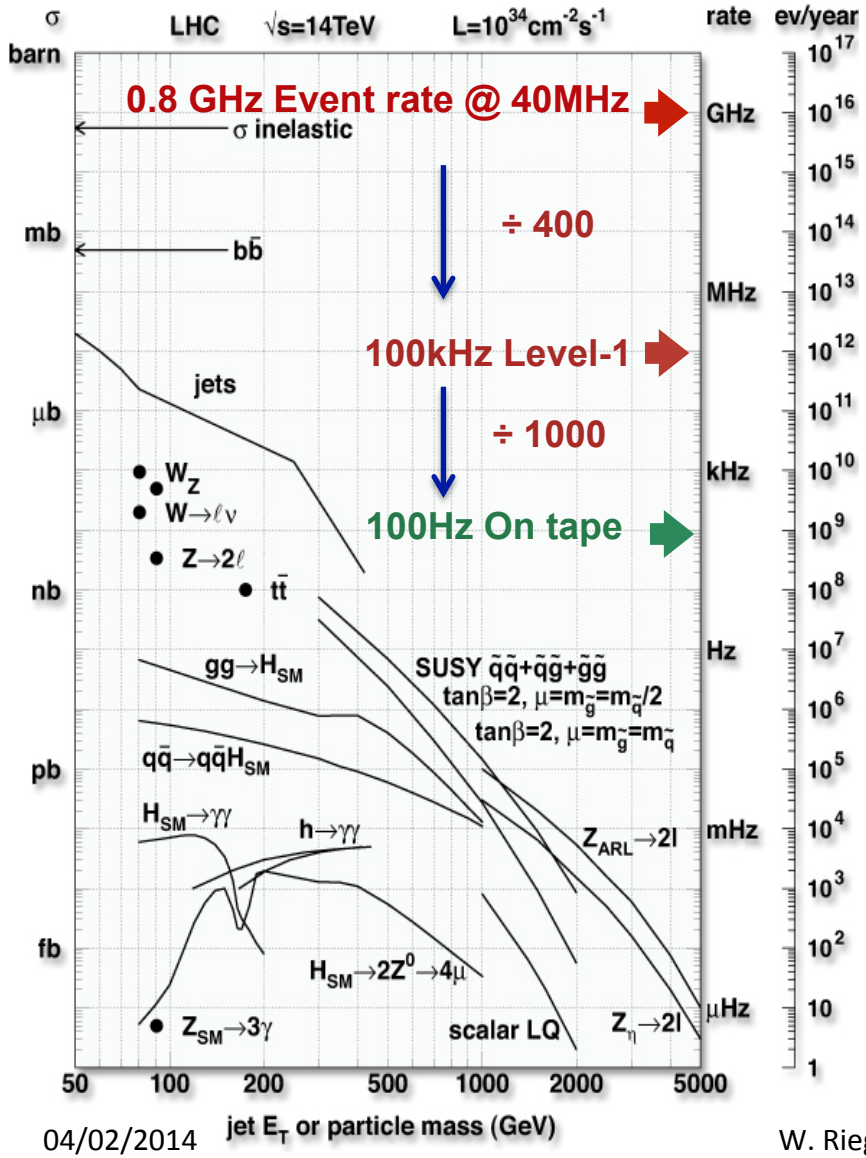

ATLAS/CMS plans for L=5x10^{34}

4 GHz Event Rate @ 40MHz

÷ 40

0.5-1 MHz Level-1 Rate

÷ 100

5-10kHz Rate to Tape

Increase in computing power, according to Moores Law doubling every 2 years, and related increase in storage capacity, makes it possible !

ATLAS & CMS @ HL-LHC (2025-2026)

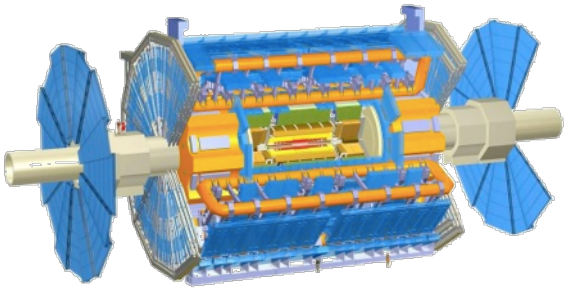

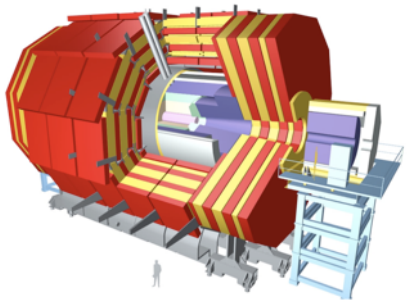

Hardware trigger to reduce events rate by factor 40

40 MHz

Level 1

0.5-1 MHz

HLT

5-10 kHz (2MB/event)

Storage

10-20 GB/s

Level 1

HLT

10 kHz (4MB/event)

Storage

40 GB/s

← PEAK OUTPUT →

ALICE & LHCb in LS2 (2019-2020)

No Hardware trigger, all data into HLT !

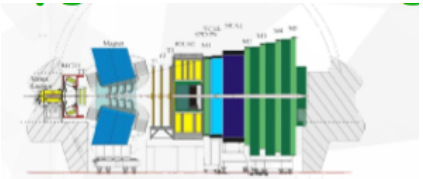

40 MHz

DAQ

40 MHz

LLT: μ,e/γ, hadrons

5-40 MHz

HLT: event recon.

20 kHz (0.1 MB/event)

Storage

2 GB/s

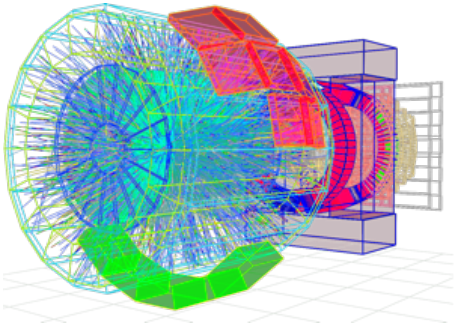

50 kHz

Reconstruction + Compression

50 kHz (1.5 MB/event)

Storage

75 GB/s

← PEAK OUTPUT →

Moore‘s Law

http://www.livescience.com/23074-future-computers.html

“If the doubling of computing power every two years continues to hold, then by 2030 whatever technology we're using will be sufficiently small that we can fit all the computing power that's in a human brain into a physical volume the size of a brain”,

explained Peter Denning, distinguished professor of computer science at the Naval Postgraduate School and an expert on innovation in computing.

"Futurists believe that's what you need for artificial intelligence. At that point, the computer starts thinking for itself.“

→ **Computers will anyway by themselves figure out what to do with the data by 2035.**

Micro Pattern Gas Detectors

MICRO-GROOVE CHAMBER

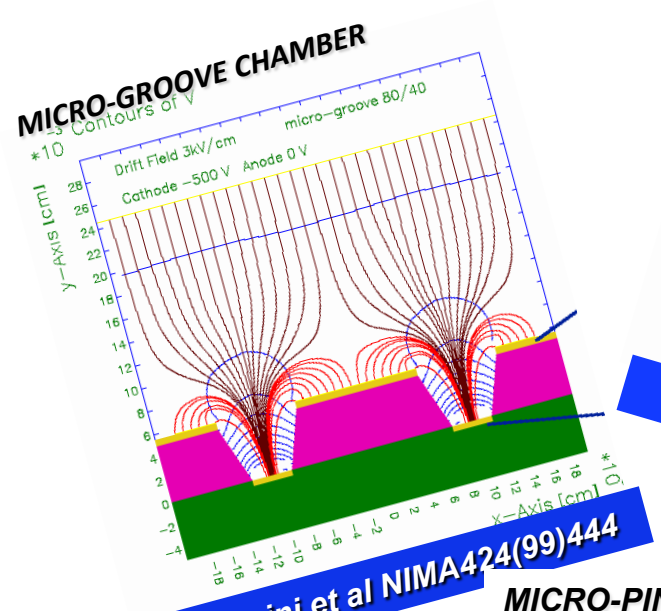

Bellazzini et al NIMA424(99)444

MICROWIRE CHAMBER

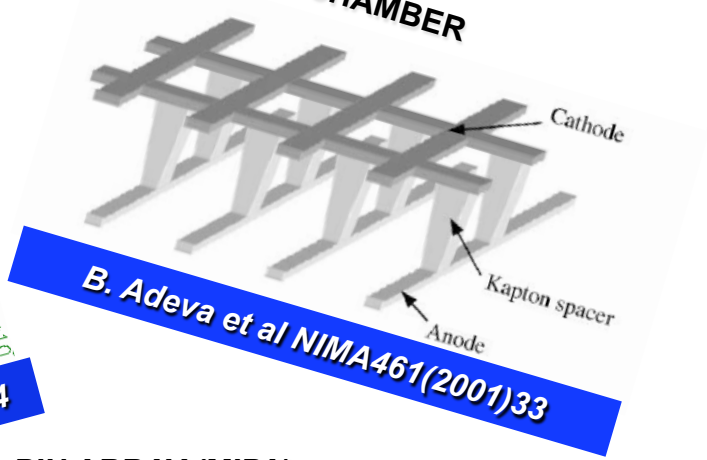

B. Adeva et al NIMA461(2001)33

MICRO-PIXEL CHAMBER

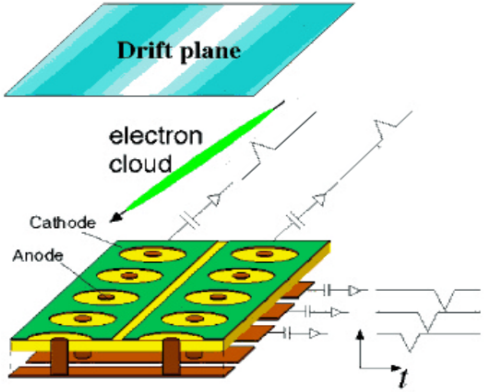

Ochi et al NIMA471(2001)264

MICRO-PIN ARRAY (MIPA)

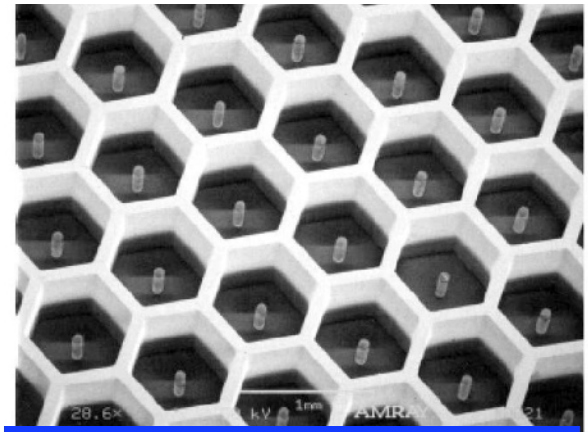

P. Rehak et al TNS NS47(2000)1426

FIELD GRADIENT LATTICE DETECTOR (FGLD)

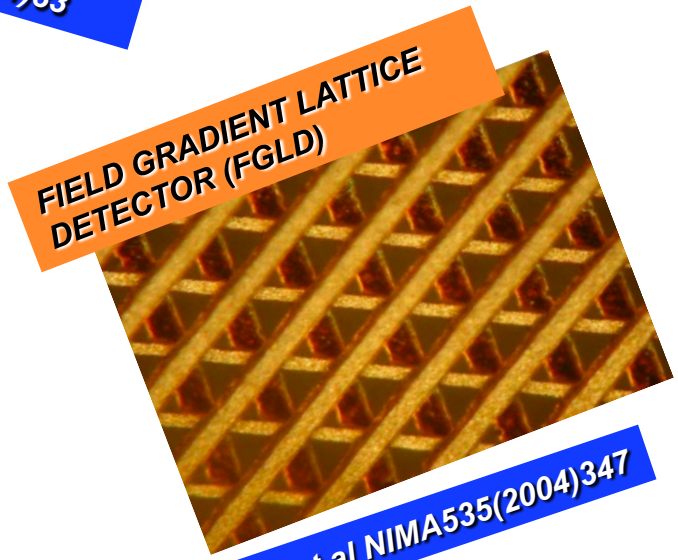

L.Dick et al NIMA535(2004)347

Micro Pattern Gas Detectors

MICROMEGA | **MSGC** | **GEM**

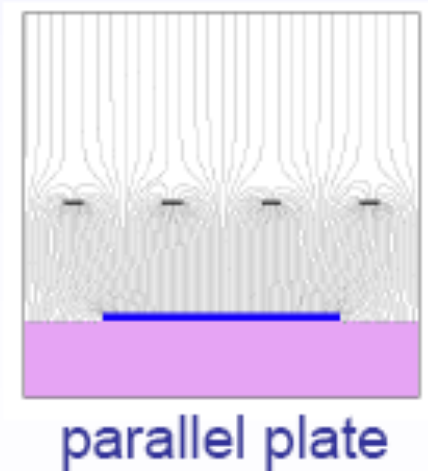

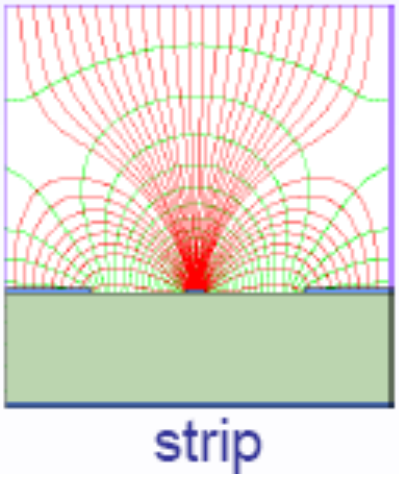

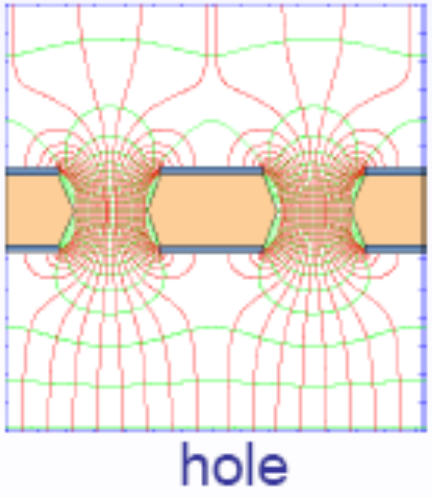

MicroMeshGasdetector | **MicroStripGasChamber** | **GasElectronMultiplier**

Note:
Wire Chambers are still very practical detectors, with high electric field only on the wire surface, well defined potentials in the entire detector volume and not extremely demanding in terms of construction cleanness etc.

Scaling Technologies

Scaling new Technologies to Large Surface Applications takes significant time and effort. Example: COMPASS GEMs and MICROMEGAS.

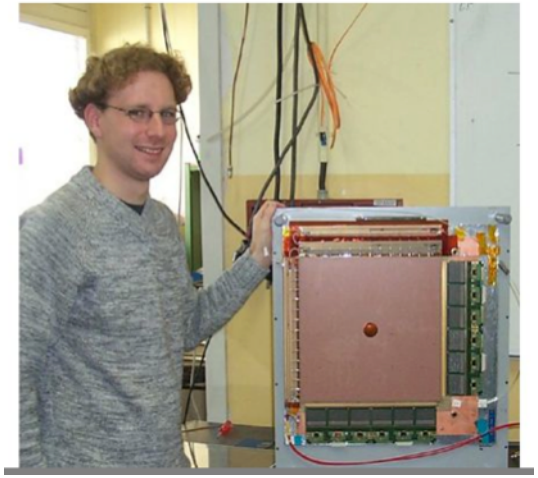

These technologies are only now applied at the LHC on a large scale (LHCb GEMs and Totem GEMs are still relatively small scale).

ALICE TPC upgrade:	100m^2 of 4-GEM detectors
CMS Muon System upgrade:	100m^2 of triple GEM detectors in LS2
ATLAS New Small Wheel:	8 planes of MICROMEGAS with total area of 1200m^2

Scaling Technologies, CMS Phase1 (2019-2020)

CMS Muon System upgrade with GEMs:

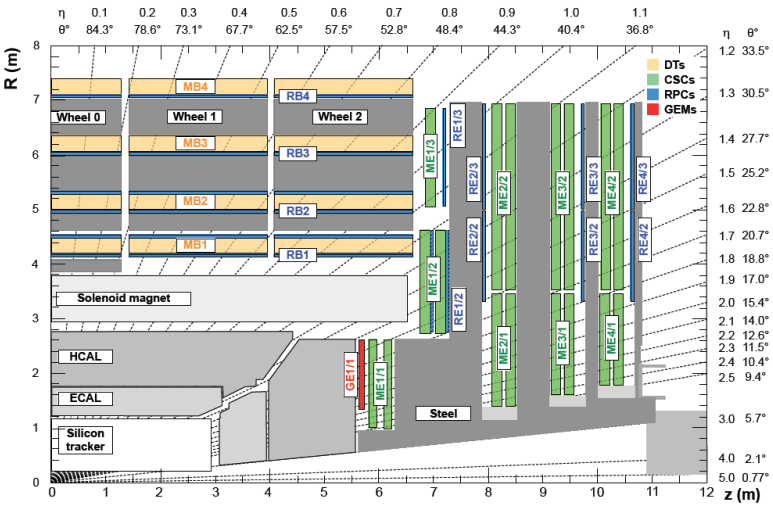

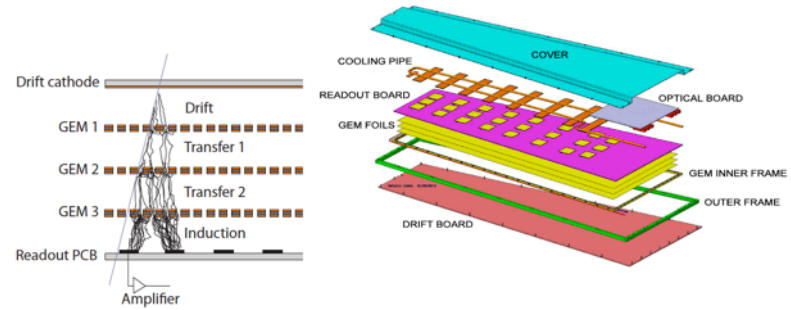

Figure 1.3: *Left:* By cascading three GEM foils, the amplification per stage can be kept modest to avoid electric breakdown problems. *Right:* Exploded view of the mechanical design of a Triple-GEM chamber.

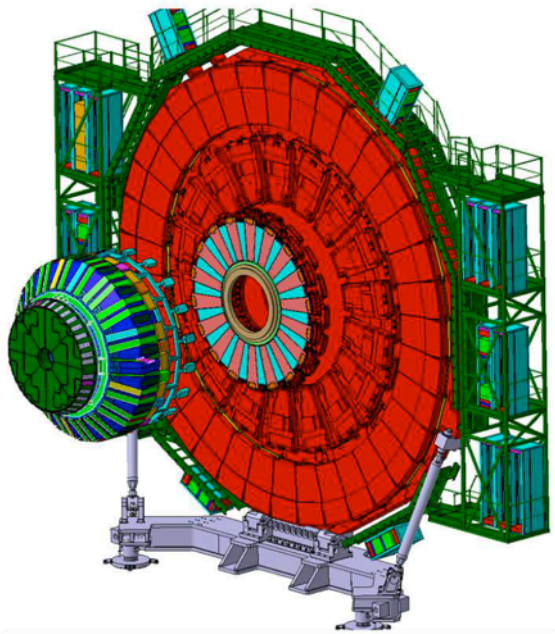

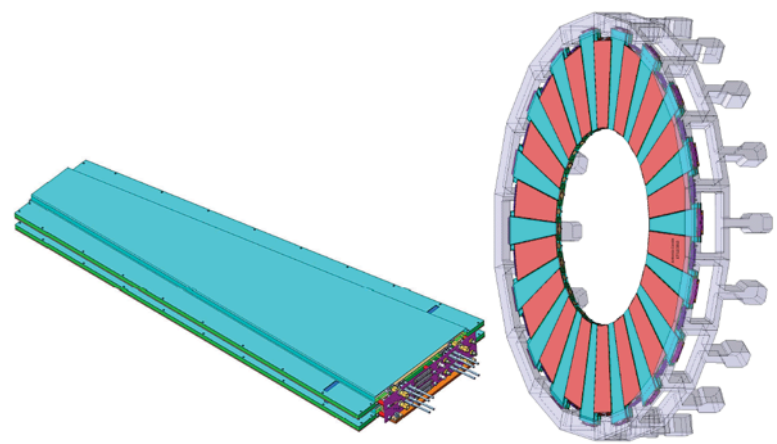

Figure 1.4: *Left:* A pair of GEM chambers form a superchamber. *Right:* Long and short chambers are combined to maximize the instrumentation within given mechanical constraints in the endcap.

Scaling Technologies, ATLAS Phase1 (2019-2020)

ATLAS Muon System upgrade with MICROMEGAs: New Small Wheel

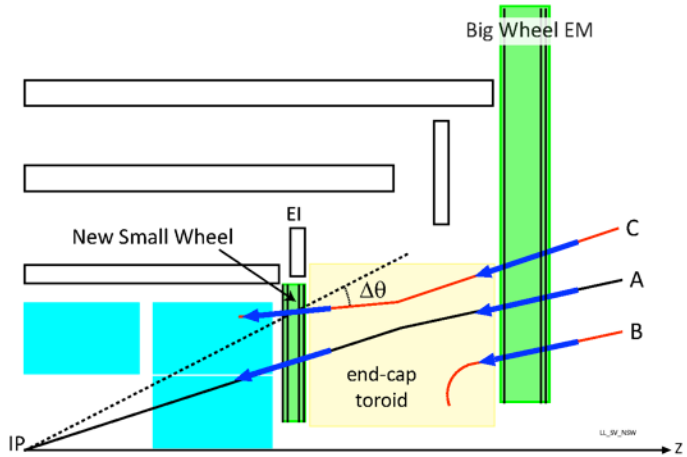

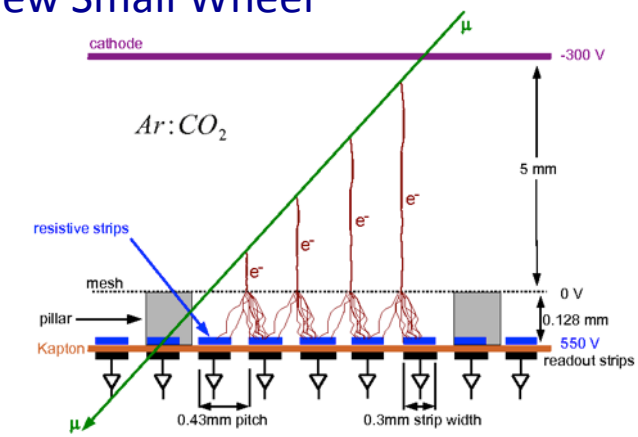

Improved stability by resistive layer on top of the readout strips.

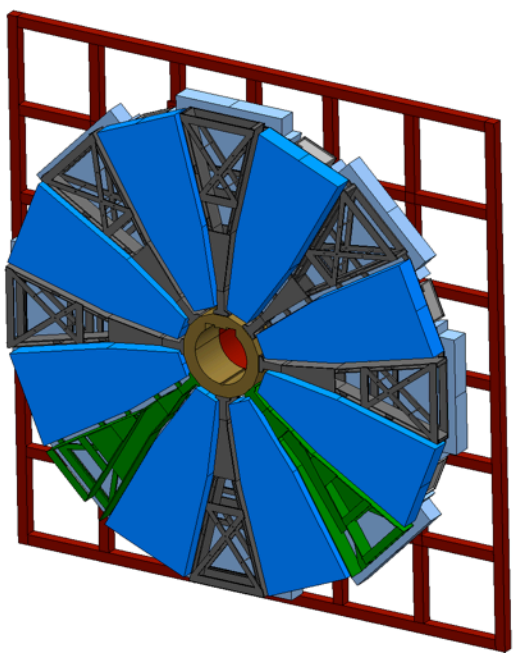

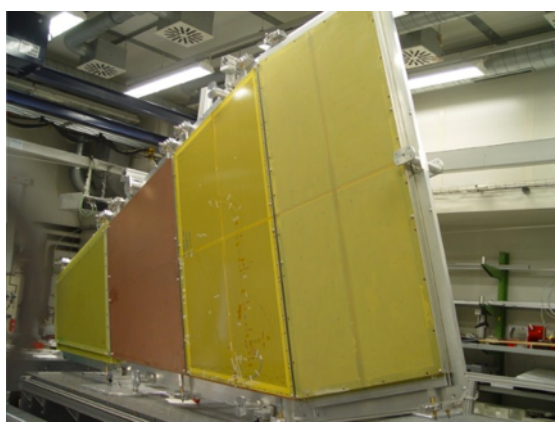

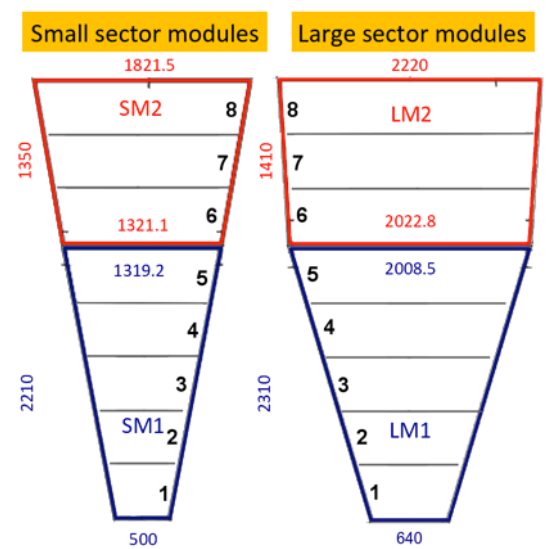

Signals in Detectors with Resistive Elements

Electric fields, weighting fields, signals and charge diffusion in detectors including resistive materials

W. Riegler, CERN

CERN EP, CH-1211 Geneve 23

arXiv:1602.07949v1 [physics.ins-det] 25 Feb 2016

Abstract

In this report we discuss static and time dependent electric fields in detector geometries with an arbitrary number of parallel layers of a given permittivity and weak conductivity. We derive the Green's functions i.e. the field of a point charge, as well as the weighting fields for readout pads and readout strips in these geometries. The effect of 'bulk' resistivity on electric fields and signals is investigated. The spreading of charge on thin resistive layers is also discussed in detail, and the conditions for allowing the effect to be described by the diffusion equation is discussed. We apply the results to derive fields and induced signals in Resistive Plate Chambers, Micromega detectors including resistive layers for charge spreading and discharge protection as well as detectors using resistive charge division readout like the MicroCAT detector. We also discuss in detail how resistive layers affect signal shapes and increase crosstalk between readout electrodes.

Keywords: RPC, Micromega, MicroCat, electric fields, weighting fields, signals, charge diffusion
PACS: 29.40.Cs, 29.40.Gx

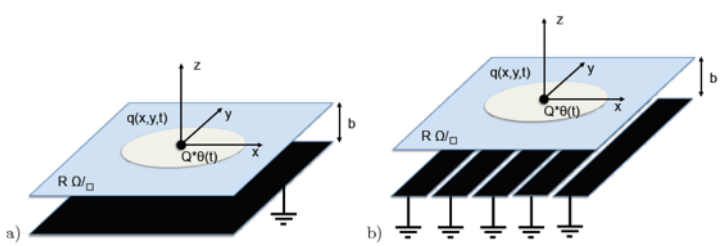

Figure 22: a) A point charge Q placed on an infinitely extended resistive layer in presence of a grounded layer. b) In case the ground plane is segmented, the time dependent charge distribution $q(r,t)$ does induce charges on the strips.

8. Signals and charge spread in detectors with resistive elements

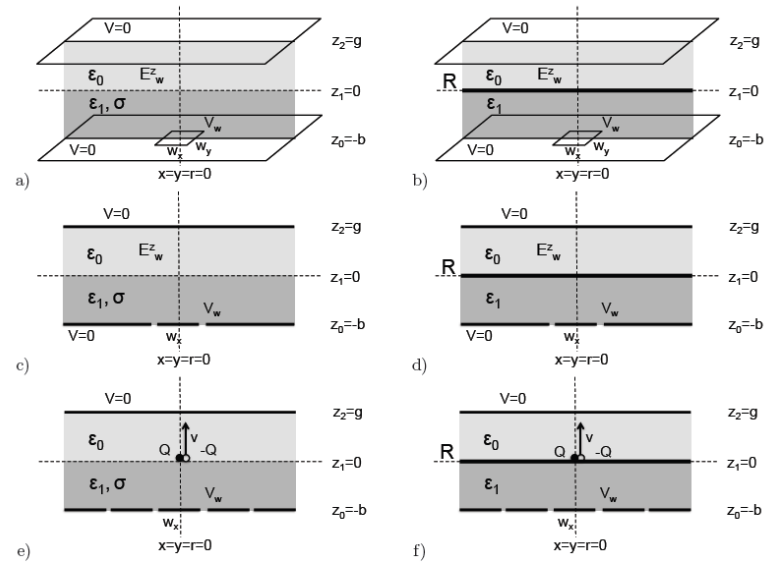

Figure 27: Weighting field for a geometry with a resistive layer having a bulk resistivity of $\rho = 1/\sigma[\Omega\text{cm}]$ (left) and a geometry with a thin resistive layer of value $R\,[\Omega/\text{square}]$ (right).

Available online at www.sciencedirect.com
SCIENCE DIRECT®
ELSEVIER
Nuclear Instruments and Methods in Physics Research A 535 (2004) 287–293
NUCLEAR INSTRUMENTS & METHODS IN PHYSICS RESEARCH Section A
www.elsevier.com/locate/nima

Extended theorems for signal induction in particle detectors VCI 2004

W. Riegler*
CERN, PH Division, Rt. De Meyrin, Geneva 23CH-1211, Switzerland

Available online 13 August 2004

ELSEVIER
Nuclear Instruments and Methods in Physics Research A 491 (2002) 258–271
NUCLEAR INSTRUMENTS & METHODS IN PHYSICS RESEARCH Section A
www.elsevier.com/locate/nima

Induced signals in resistive plate chambers

Werner Riegler
EP Division, CERN, CH-1211 Geneva 23, Switzerland

Received 10 April 2002; received in revised form 30 April 2002; accepted 2 May 2002

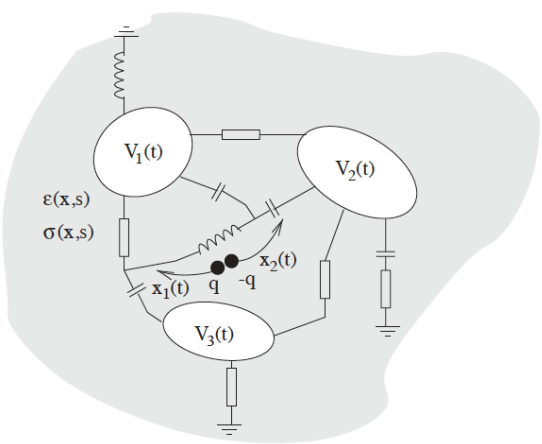

Fig. 1. At $t = 0$ a pair of charges is created at a space point from where they move along different trajectories. This movement induces voltages on the electrodes.

Electric fields, weighting fields, signals and charge diffusion in detectors including resistive materials

W. Riegler
CERN EP,
CH-1211 Geneve 23, Switzerland
E-mail: werner.riegler@cern.ch

Abstract: In this report we discuss static and time dependent electric fields in detector geometries with an arbitrary number of parallel layers of a given permittivity and weak conductivity. We derive the Green's functions i.e. the field of a point charge, as well as the weighting fields for readout pads and readout strips in these geometries. The effect of 'bulk' resistivity on electric fields and signals is investigated. The spreading of charge on thin resistive layers is also discussed in detail, and the conditions for allowing the effect to be described by the diffusion equation is discussed. We apply the results to derive fields and induced signals in Resistive Plate Chambers, MICROMEGAS detectors including resistive layers for charge spreading and discharge protection as well as detectors using resistive charge division readout like the MicroCAT detector. We also discuss in detail how resistive layers affect signal shapes and increase crosstalk between readout electrodes.

Keywords: Charge induction; Detector modelling and simulations II (electric fields, charge transport, multiplication and induction, pulse formation, electron emission, etc); Micropattern gaseous detectors (MSGC, GEM, THGEM, RETHGEM, MHSP, MICROPIC, MICROMEGAS, InGrid, etc); Resistive-plate chambers

ArXiv ePrint: 1602.07949

2016 JINST 11 P11002

Scaling Technologies, ALICE Phase1 (2019-2020)

PbPb collision rate will increase from 10kHz to 50kHz.
With 100us drift time, classical wire chamber gating will not work
→ build a continuously sensitive TPC with GEMs

A Large Ion Collider Experiment

ALICE

THE ALICE TPC

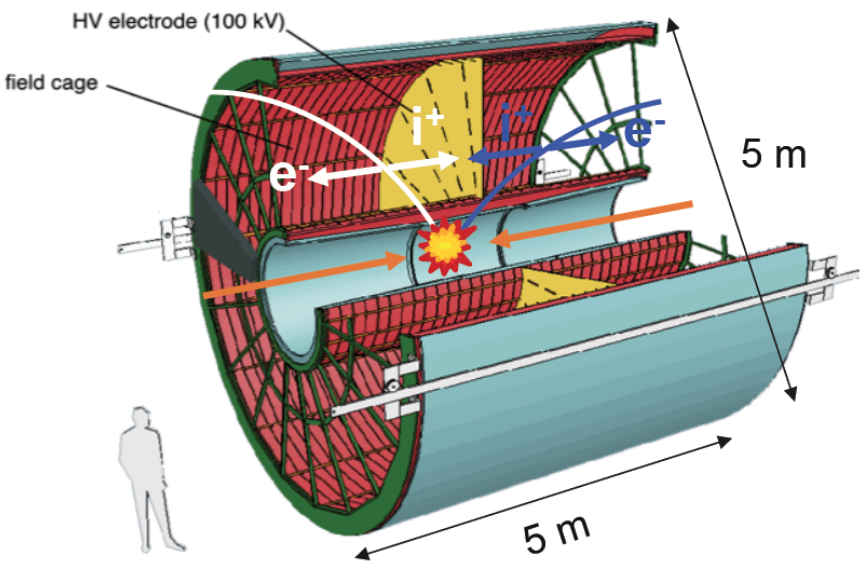

Gas volume

- Acceptance: $|\eta|<0.9$, $\Delta\phi = 2\pi$
- Low mass, high precision field cage
- ~90 m^3 active detector medium

- Gas:
  - Ne-CO_2 (90-10) in RUN 1
  - Ar-CO_2 (90-10) in RUN 2

- 100 kV at the Central Electrode
  - E_{drift} = 400 V/cm
  - v_{drift} = 2.7 cm/μs
  - max t_{drift} = 92 μs

Scaling Technologies, ALICE Phase1 (2019-2020)

THE ALICE TPC

2 x 18 Outer Read Out Chambers

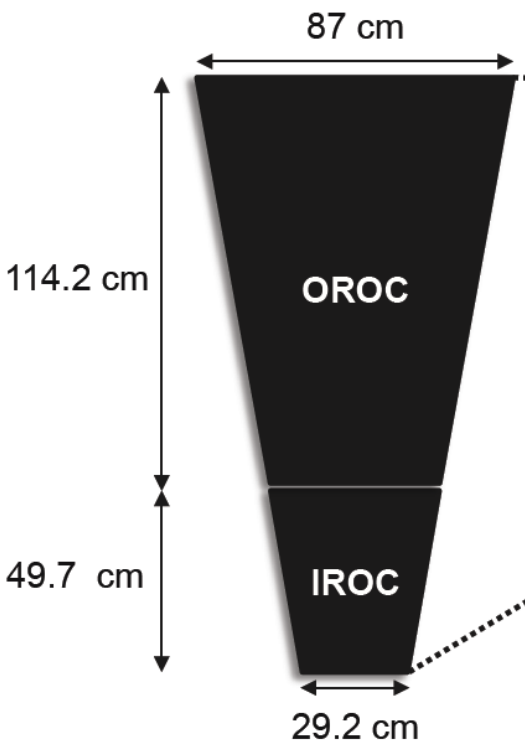

557,568 pads (159 rows)

4 x 7.5 mm^2	(IROC)
6 x 10 mm^2	(OROC)
6 x 15 mm^2	(OROC)

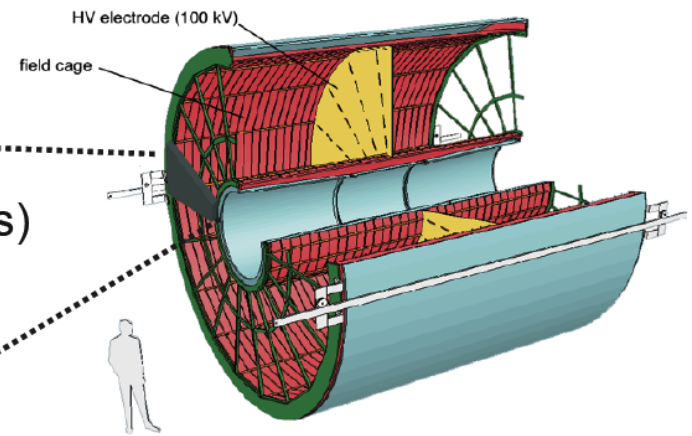

2 x 18 Inner Read Out Chambers

Readout chambers

- 72 MWPCs with pad readout
- $\sigma_{dE/dx}$ = 5.5% (7%) in p-p (Pb-Pb)
- Gating grid

Scaling Technologies, ALICE Phase1 (2019-2020)

A Large Ion Collider Experiment

ALICE

BASELINE SOLUTION: 4-GEM SETUP

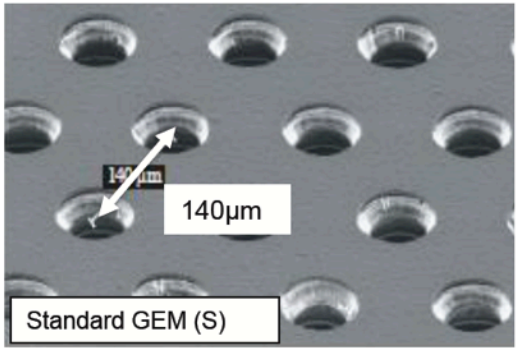

- Requirements not fullfilled with a standard 3-GEM configuration
- New readout chambers employ standard (S) and large-pitch (LP) GEMs in a configuration S-LP-LP-S
- Optimized HV settings

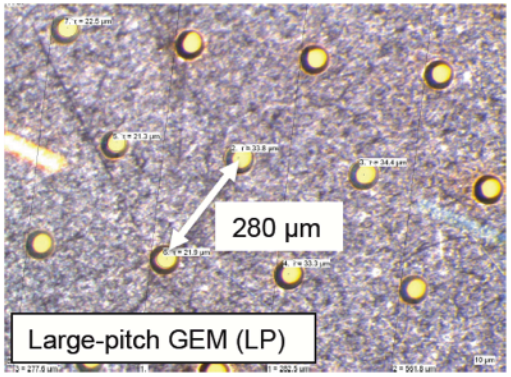

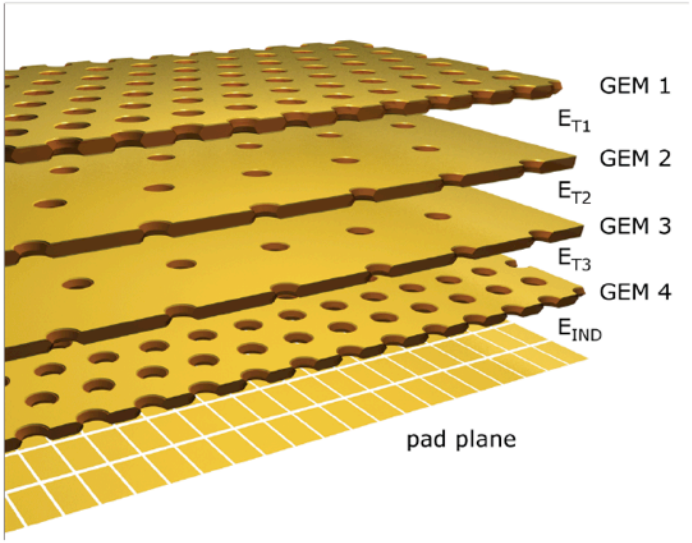

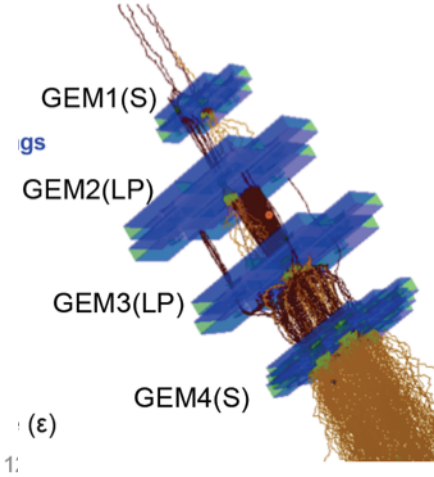

HV SETTINGS OPTIMIZATION

- "Standard" HV settings used with GEM detectors (e.g. COMPASS) not optimal for low IBF
- IBF optimized settings:
  - $\Delta_{GEM1} > \Delta_{GEM2} \approx \Delta_{GEM3} << \Delta_{GEM4}$ (largest amplification in GEM4 → stability?)
  - High E_{T1}, E_{T2} (high electron extraction from the first GEM stages)
  - Low E_{T3} (ion blocking)

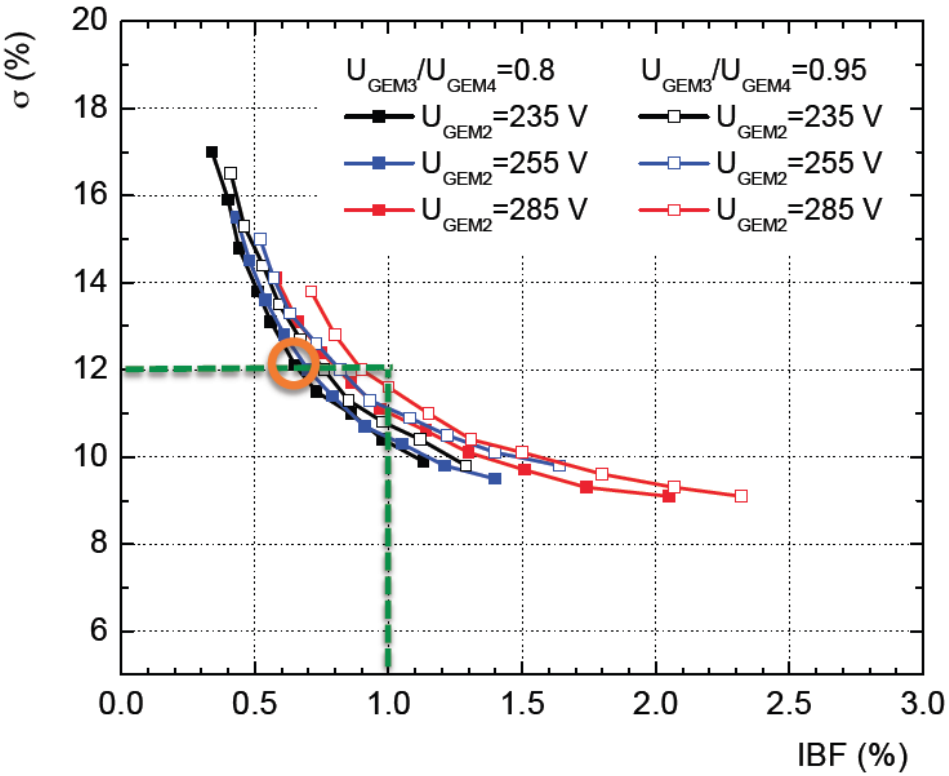

Gas mixture: Ne-CO_2-N_2 (90-10-5)

Effective gain G_{eff} = 2000

Baseline solution (S-LP-LP-S) performance:

IBF = 0.6 %

σ_E/E ≈ 12 % for 5.9 keV (^{55}Fe)

Alternative R&D:

2GEM + Micromegas

COBRA GEMs

GEMS FOR THE UPGRADE

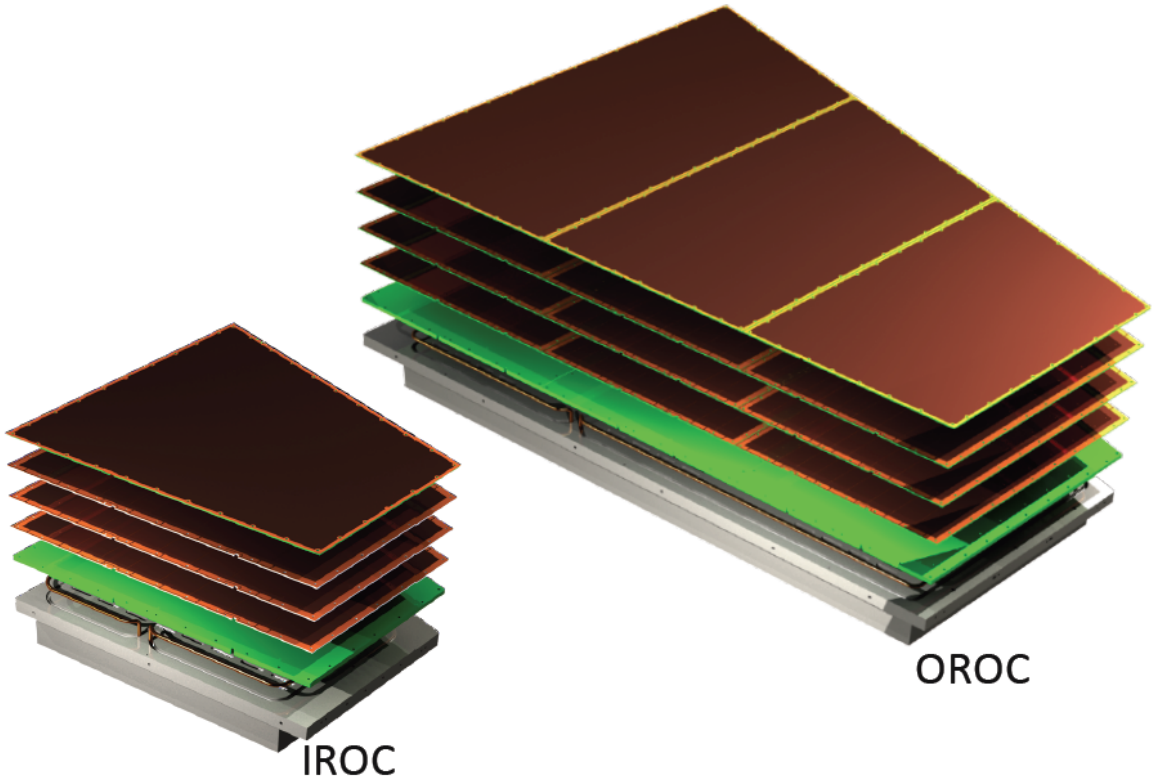

- Large-size single-mask foils from CERN PCB workshop
- 1 stack in IROC, 3 stacks in OROC

Silicon Detectors for Tracking and Calorimetry

Huge plans with silicon within HL-LHC Upgrade ...

universitätbonn

- ... largest is CMS HGC (Forward Calorimeter) — 780 m^2 silicon (pads)
- ... HL-LHC trackers of ATLAS and CMS — ~200 m^2 silicon (strips & pixels)

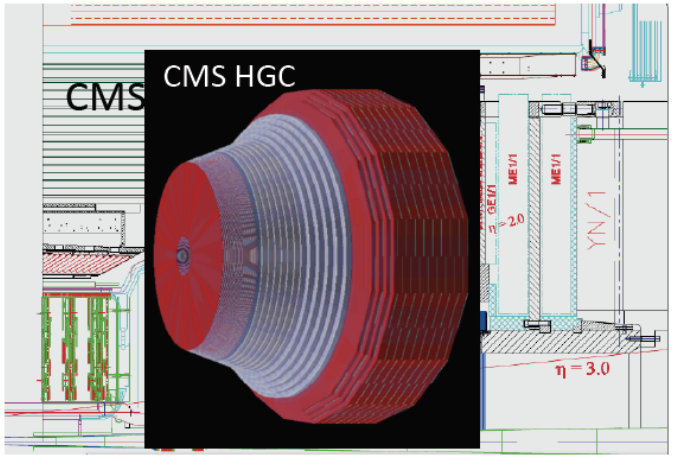

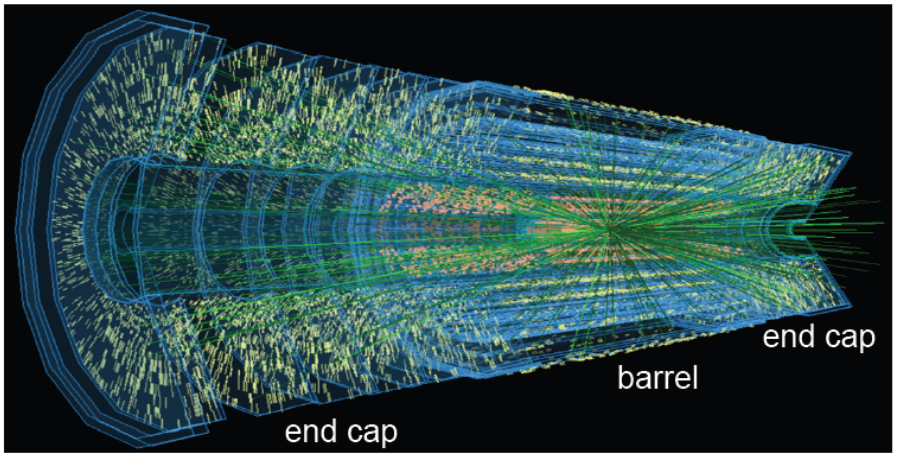

- Radiation hardness and rate performance must increase compared to LHC Run I by ...
  - phase 0 (2015) ≈ × 5
  - phase 1 (2018) ≈ × 5-10
  - phase 2 (>2025) ≈ × 10-30

- Increased luminosity (@ large area) thus demands ...
  - higher hit-rate capability
  - increased granularity
  - higher radiation tolerance
  - lighter detectors
  - cheaper price tag !!

$> 10^{16}\ n_{eq}\ cm^{-2}$

TID: > 1 Grad

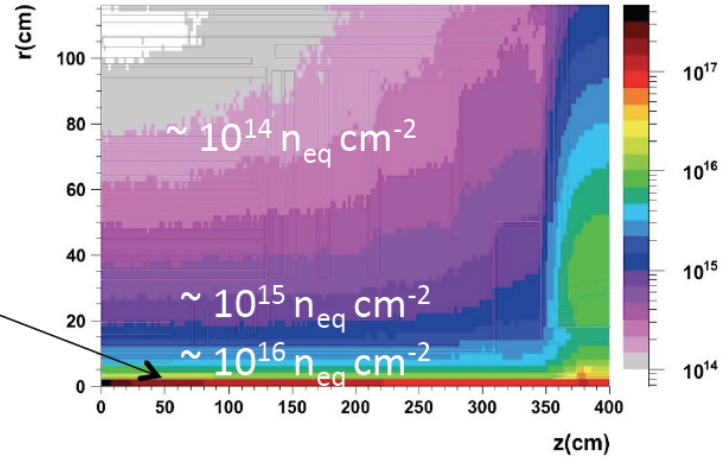

For upgrades: p-type silicon substrates

- classic strip choice: p^+ in n
- for HL upgrade: n^+ in p or n^+ in n (-> p)

after high irradiation

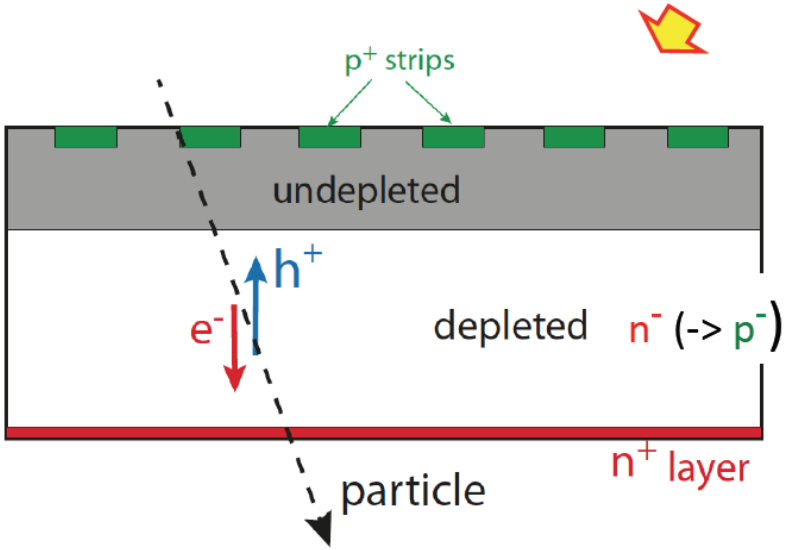

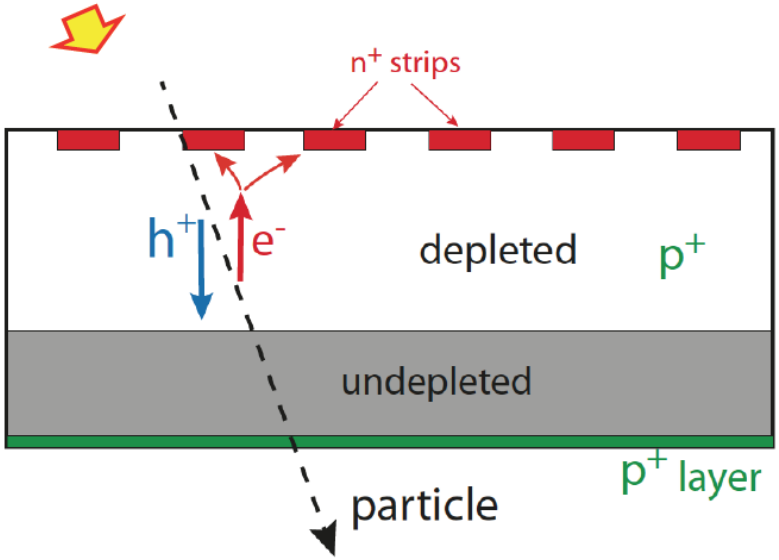

consequences:

- signal loss
- resolution degradation (Q spreading)

advantages:

- faster charge collection (electrons)
- signal and CCE degradation less&smoother

p – type substrates favoured for strips and pixels

3D-Si sensors for the innermost pixel layer(s)

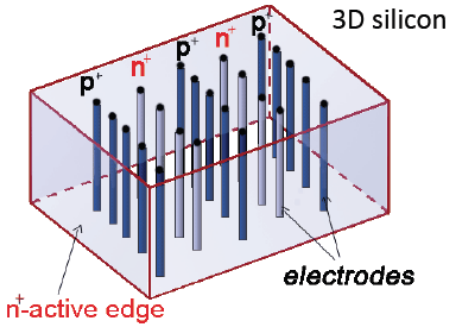

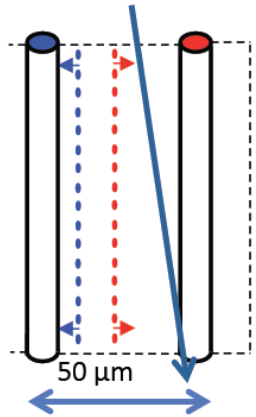

S. Parker, C. Kenney , J. Segal, ICFA Instrum.Bull. 14 (1997) 30-50
C. Da Via, et al., NIM A49 (2005) 122-125 and NIM A 699 (2013) 18

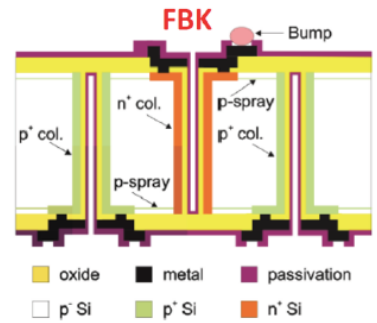

G.F. Della Betta et al.,
PoS Vertex2012 (2013) 014

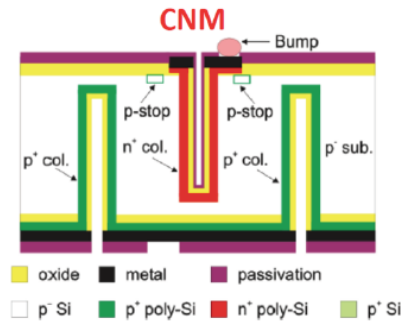

G. Pellegrini et al..
NIM A731 (2013) 198-200

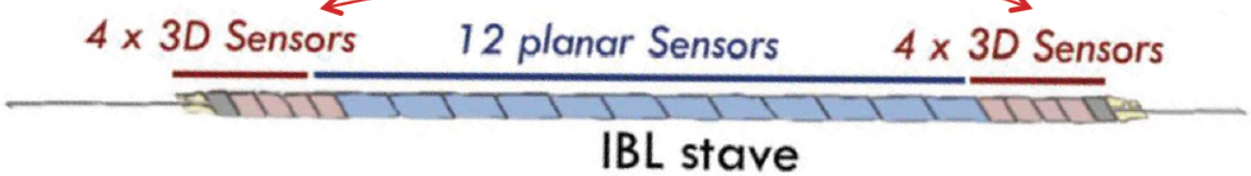

- ➢ particle path (signal) different from drift path
- ➢ high field w/ low voltage

-> radiation tolerance
-> Q still 50% @ 10^{16} cm^{-2}

- ➢ good for inclined tracks

- ▪ slightly larger C_{in} (noise)

- ✧ now also in diamond, CdTe

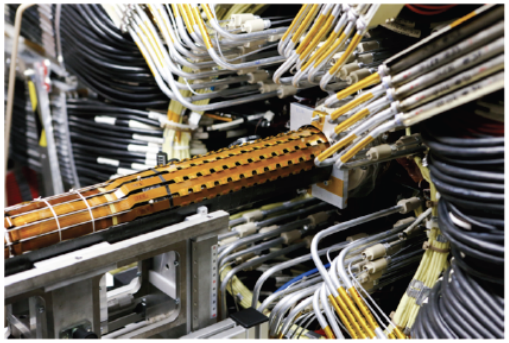

- ▪ 3D sensors have been put to reality
- ▪ in ATLAS IBL for one year
- ▪ Let's see how they performed

see also dedicated talk by Didier Ferrere

Typical pre-TDR favourite views ...

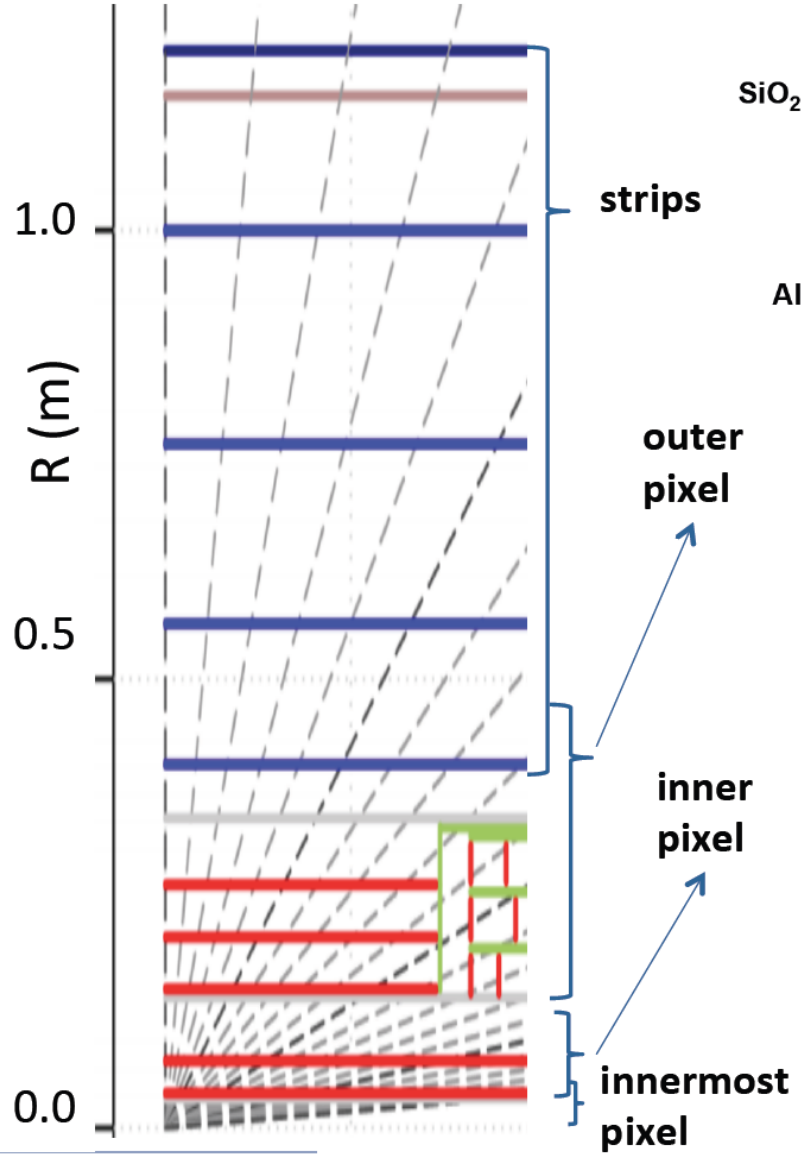

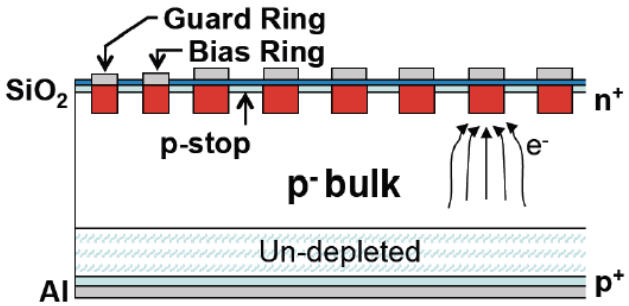

n in p
strip modules

depl. CMOS pixels

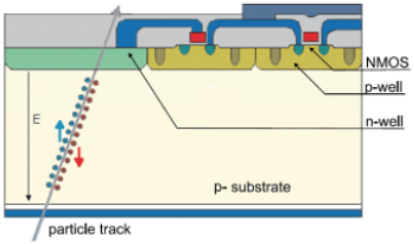

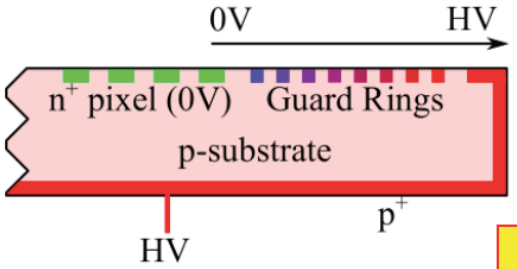

large modules
planar n in p pixels / CMOS?

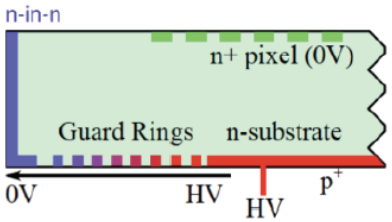

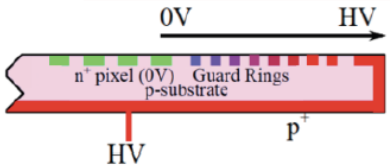

3D silicon

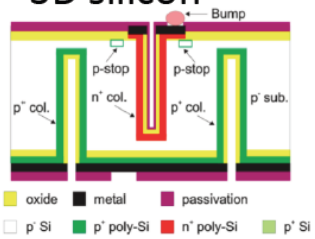

dedicated
rad.-hard
detectors

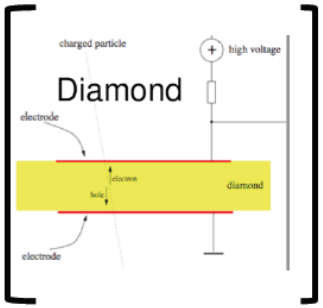

From HYBRID to monolithic CMOS pixels

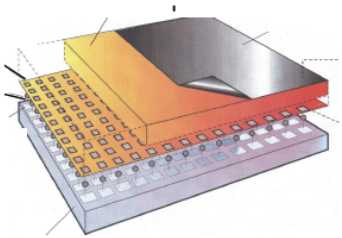

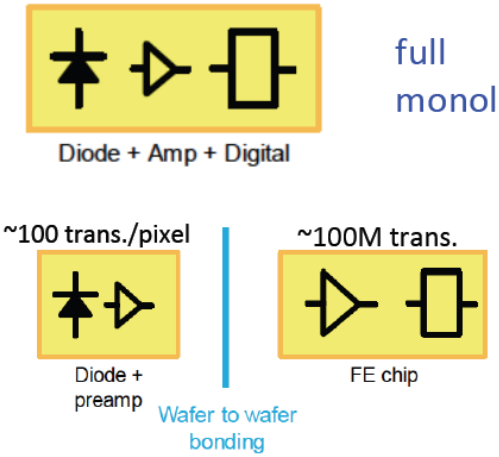

Monolithic Active Pixel Sensors

B. Dierickx, D. Meynants, G. Scheffer, SPIE 3410:68-76 (1998)
R. Turchetta, …, M. Winter et al, NIM A458 (2001) 677-689

- **MAPS** using CMOS with Q-collection in **epi**-layer: developed for > 10 yrs
  Q by <u>diffusion</u> → recent advances

- Depleted **DMAPS** (CMOS pixels)
  - using **HR** substrates and **HV** add-ons to create some depletion region
  - CMOS on **SOI**

STAR + ALICE

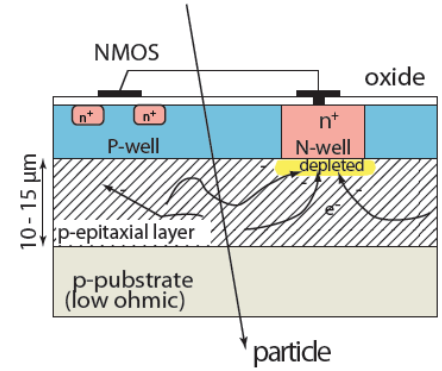

HL - LHC

$$d \sim \sqrt{\rho \cdot V}$$

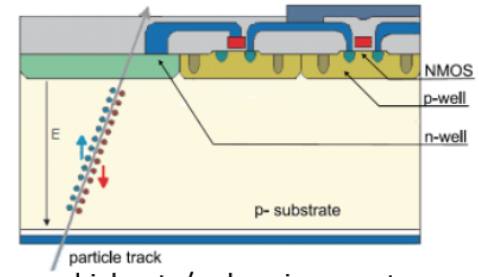

high rate/rad environment

MAPS-Pixels of the STAR detector @ RHIC

universitätbonn

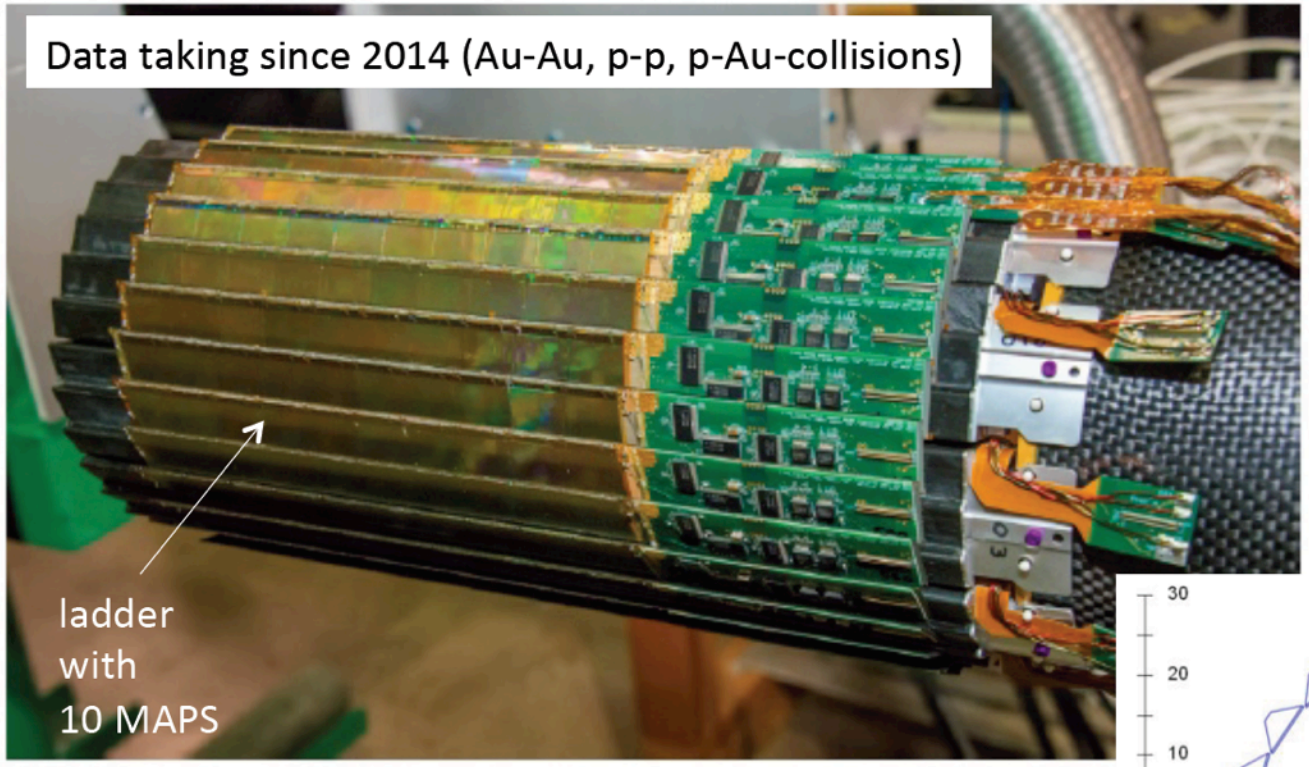

356 M pixels
in 2 layers
~0.16 m^2

Features

- 20.7 x 20.7 μm^2 pixels
- rolling shutter R/O
- signal ~1000 e-
- S/N ~ 30
- 0.39 % X/X_0

- < 90 krad / year
- < 10^{12} n_{eq}/cm^2/year

ALICE Silicon Tracker Upgrade (2019-2020)

12.5 G-pixel camera
(~10 m²)

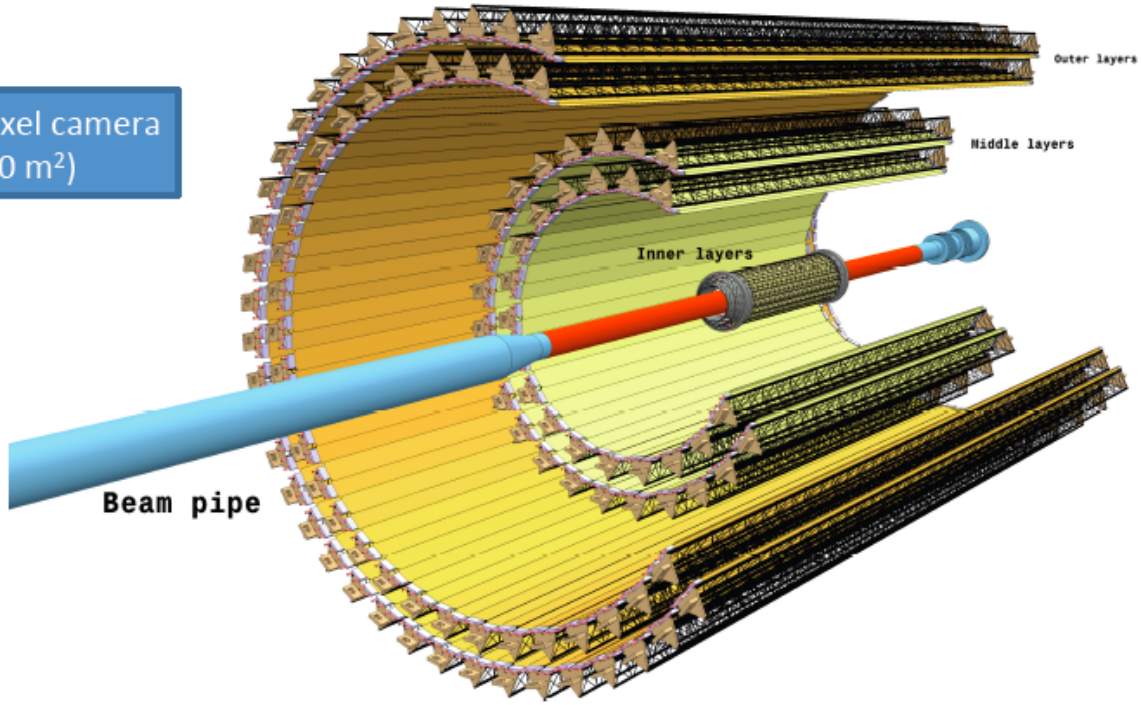

Radiation Load
- TID: ~ 270 krad
- NIEL: ~1.7×10^{12} 1MeV n_{eq} / cm^2

Design Requirements
Event Rate Readout (to tape)

Pb-Pb: 50 kHz

pp: 1 MHz

7-layer barrel geometry based on **CMOS Pixel Sensors**

r coverage: 23 – 400 mm

η coverage: $|\eta| \leq 1.22$
for tracks from 90% most luminous region

3 Inner Barrel layers (**IB**)

4 Outer Barrel layers (**OB**)

Material /layer : 0.3% X_0 (IB), 1% X_0 (OB)

L. Musa, ECFA HL-LHC workshop, Oct. 2016

ALICE Silicon Tracker Upgrade (2019-2020)

CMOS Pixel Sensor using TowerJazz 0.18μm CMOS Imaging Process

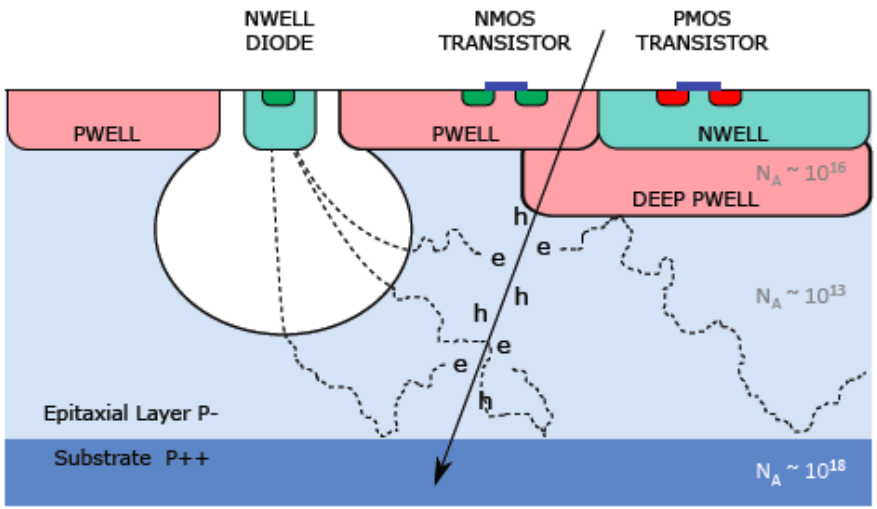

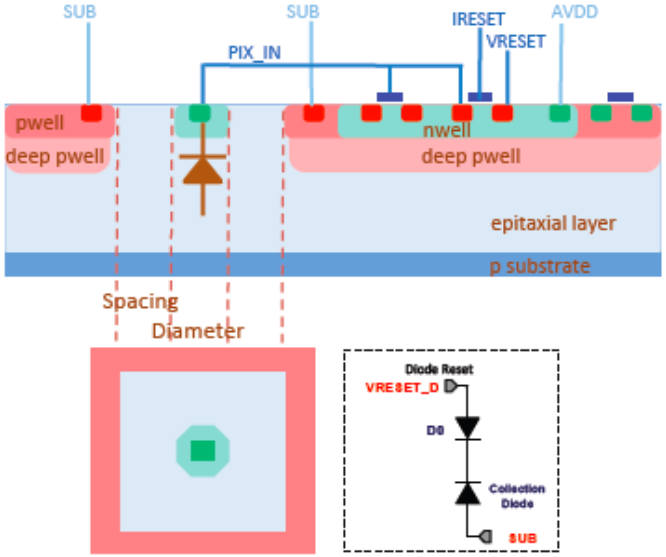

- High-resistivity (> 1kΩ cm) p-type epitaxial layer (25μm) on p-type substrate
- Small n-well diode (2 μm diameter), ~100 times smaller than pixel => low capacitance (~fF)
- Reverse bias voltage ($-6V < V_{BB} < 0V$) to substrate (contact from the top) to increase depletion zone around NWELL collection diode
- Deep PWELL shields NWELL of PMOS transistors (full CMOS circuitry within active area)

L. Musa, ECFA HL-LHC workshop, Oct. 2016

ALICE Silicon Tracker Upgrade (2019-2020)

Key Features

- Dimensions: 30mm x 15mm
- Pixel pitch: 29μm x 27μm
- Ultra-low power (entire chip): ~40mW/cm^2

Wafer probe testing

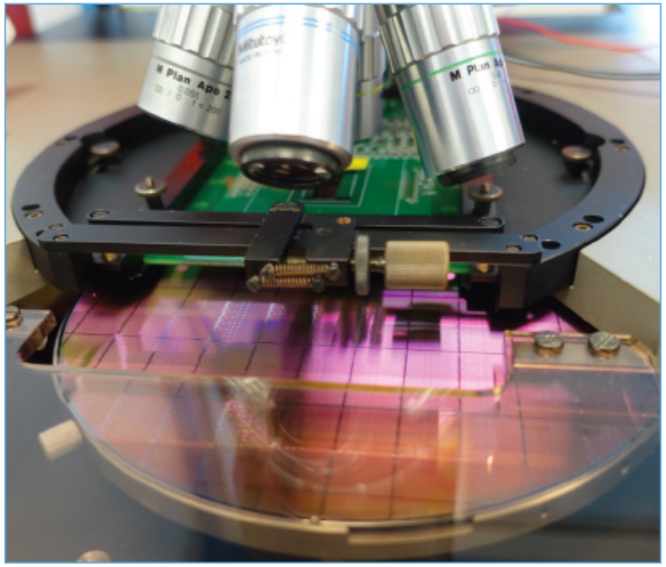

Thinned & diced wafers (chips still attached to support tape)

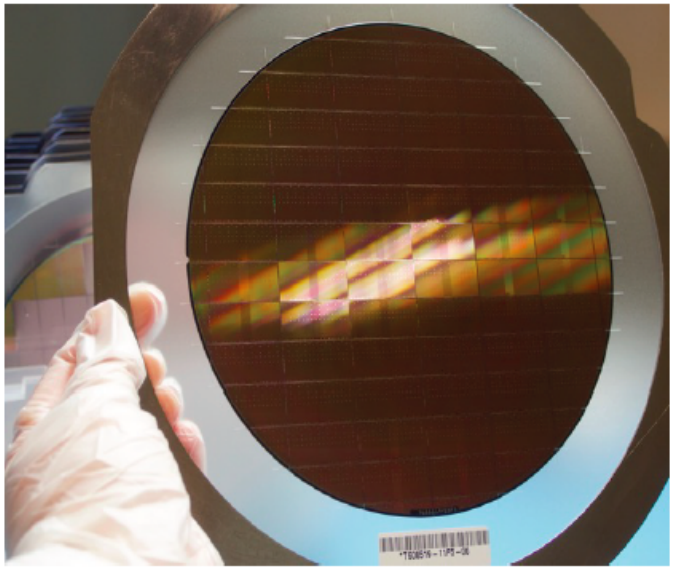

Single chips after thinning & dicing

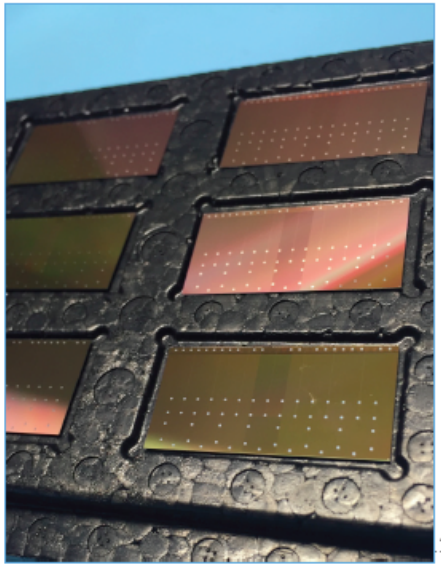

L. Musa, ECFA HL-LHC workshop, Oct. 2016

ALICE Silicon Tracker Upgrade (2019-2020)

ALPIDE – Preliminary Results

ALICE ITS Upgrade

Thresholds and Noise

S-curve scan using internal charge injection circuit

- keep comparator threshold fixed
- inject varying charges
- extract threshold and noise from error-function fit

$$P_{HIT}(q) = \frac{1}{2} \cdot Erf\left[\frac{q-\mu}{\sqrt{2}\cdot\sigma}\right]$$

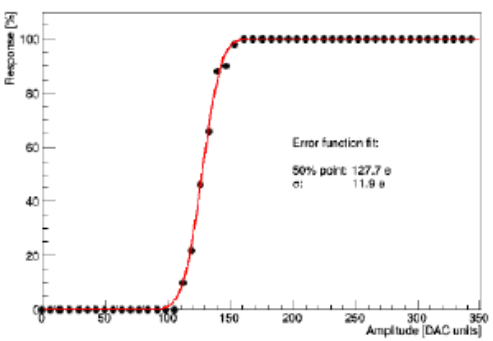

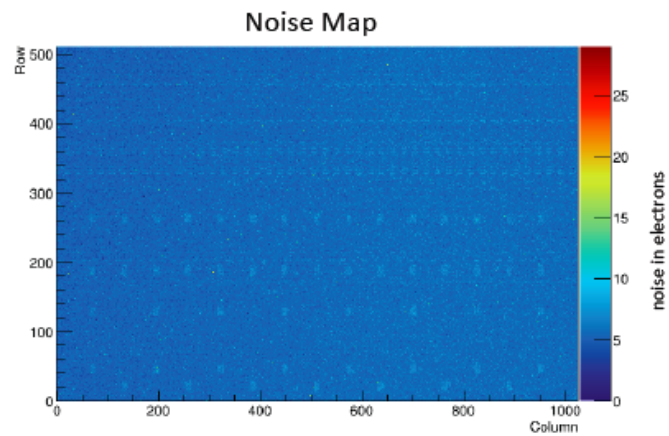

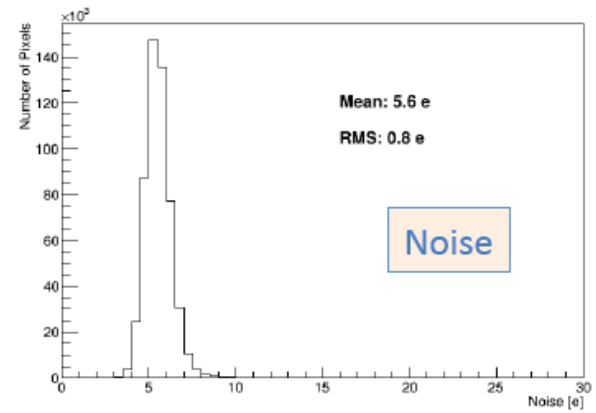

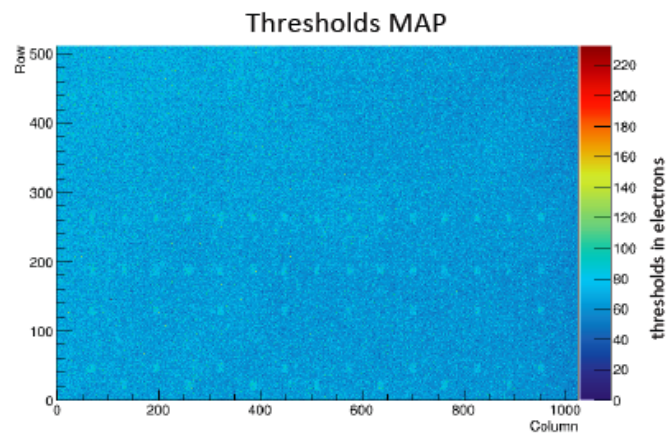

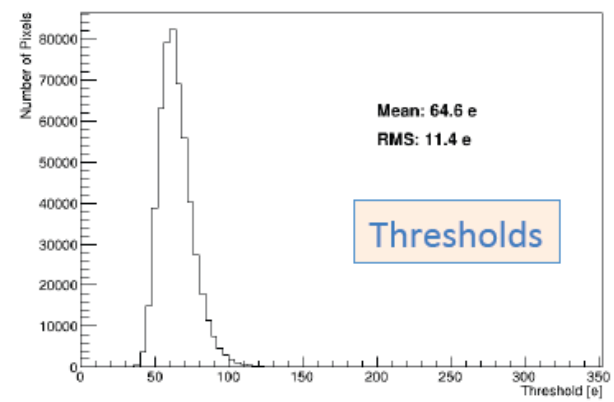

L. Musa, ECFA HL-LHC workshop, Oct. 2016

ALICE Silicon Tracker Upgrade (2019-2020)

ALPIDE – Preliminary Results

Detection Efficiency, Noise Occupancy, Cluster Size and Resolution

Test Beam (CERN PS, 6 GeV/c π) – Sep 2016

Preliminary!

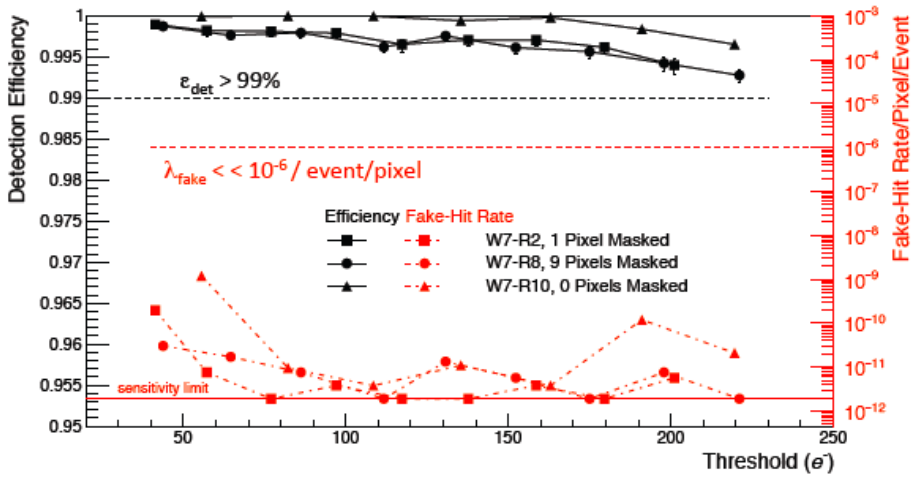

Detection efficiency & Fake Hit Rate

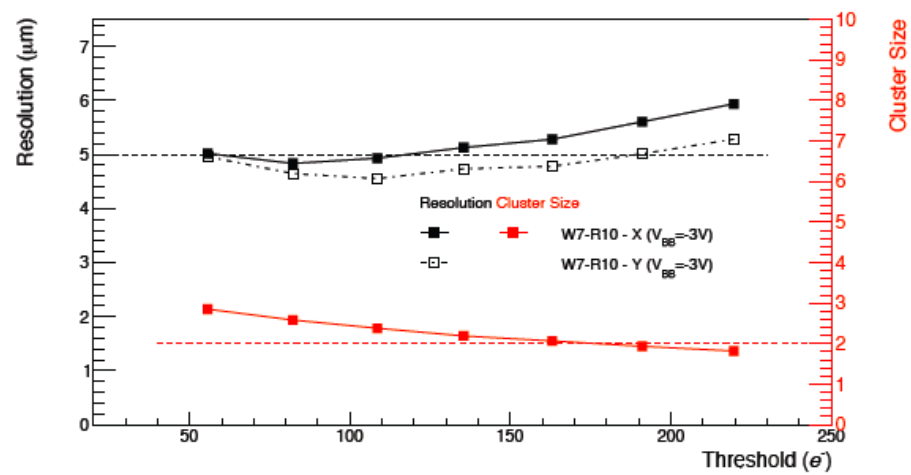

Spatial Resolution & Cluster Size

L. Musa, ECFA HL-LHC workshop, Oct. 2016

MAPS towards more Radiation Hardness

TJ Modified CIS Process

ALICE ITS Upgrade

ALICE

Standard Process

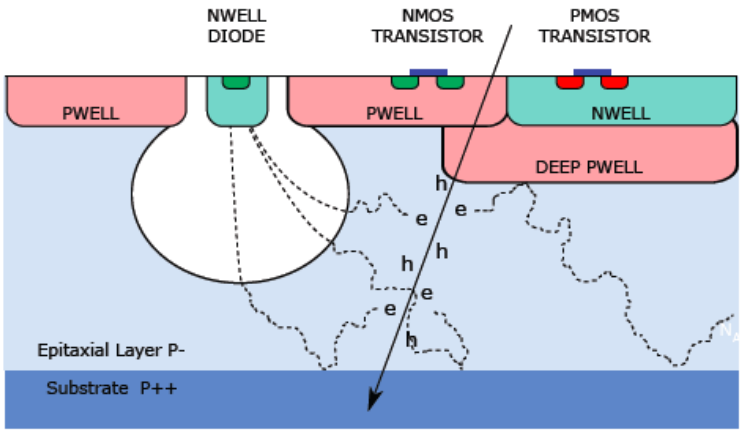

Modified Process (CERN-TJ)

Developed in collaboration with the foundry

Planar deep junction $N^- - P_{epi}$ ➔ enhanced (full?) depletion

Processed using pALPIDE2 mask set

INVESTIGATOR "test chip" also measured by ATLAS and CLIC

Note: not used for ALICE ITS Upgrade

L. Musa, ECFA HL-LHC workshop, Oct. 2016

MAPS towards more Radiation Hardness

TJ standard process vs modified process - performance after 1e15 n_{eq}

ALICE ITS Upgrade

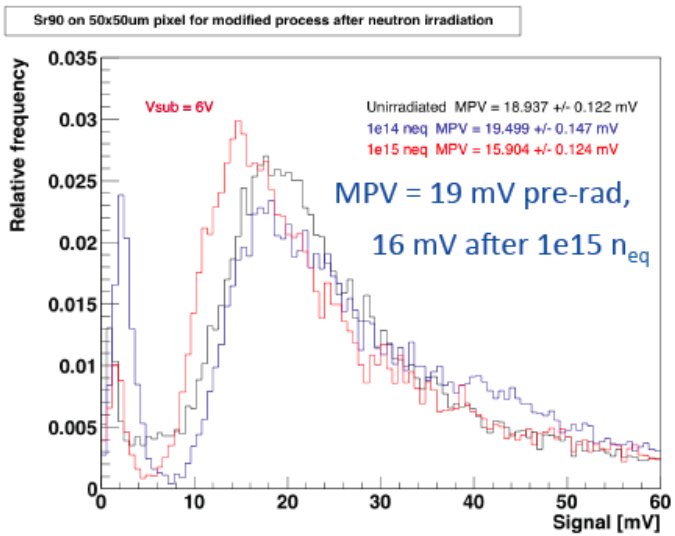

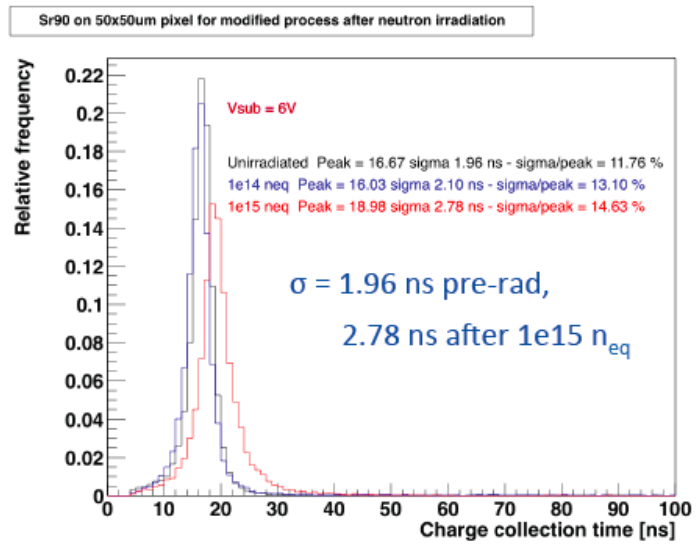

Courtesy of H. Pernegger (ATLAS)

Detection efficiency measurements in progress, first results encouraging

Standard process not working after 1e15 n_{eq}

L. Musa, ECFA HL-LHC workshop, Oct. 2016

Silicon Photomultipliers

Solid-state … Geiger mode Avalanche Photodiode (G-APD)

How to obtain higher gain (= single photon detection) without suffering from excessive noise ?

Operate APD cell in Geiger mode (= full discharge), however with (passive) quenching.

Photon conversion + avalanche short-circuits the diode.

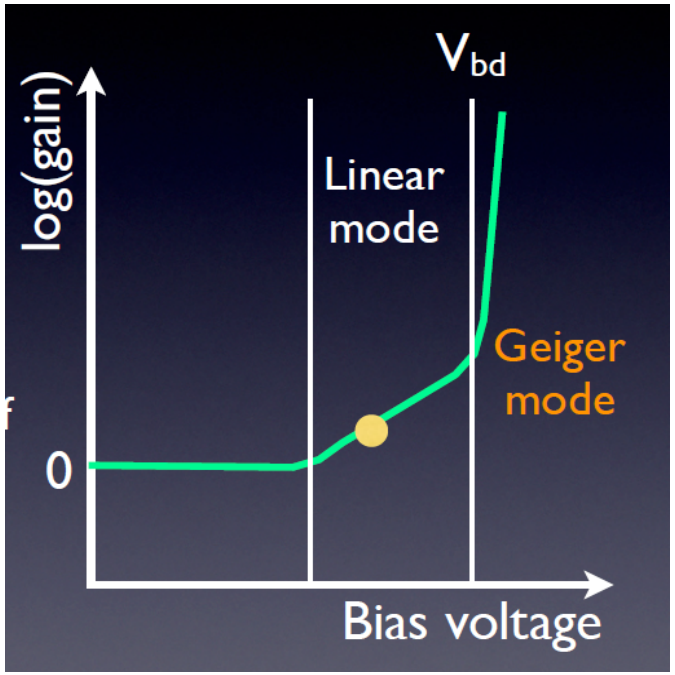

J. Haba, RICH2007

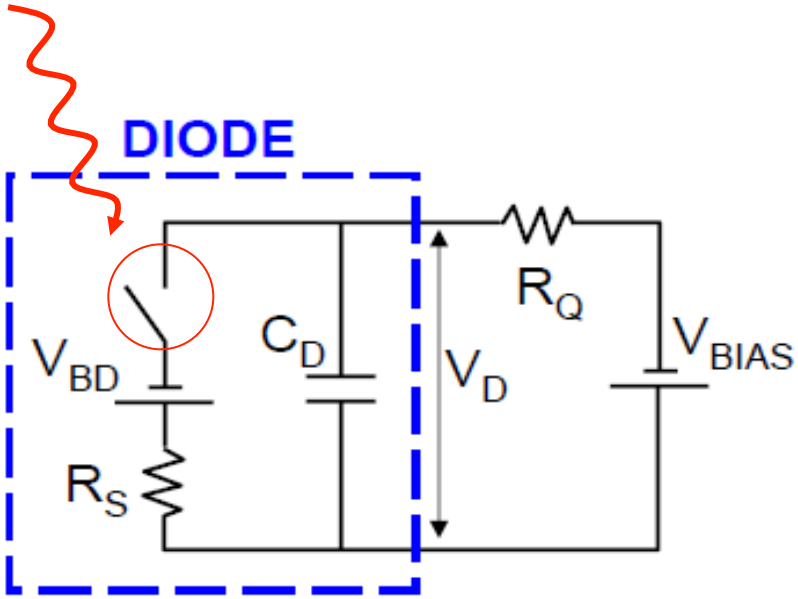

J. Haba, RICH2007

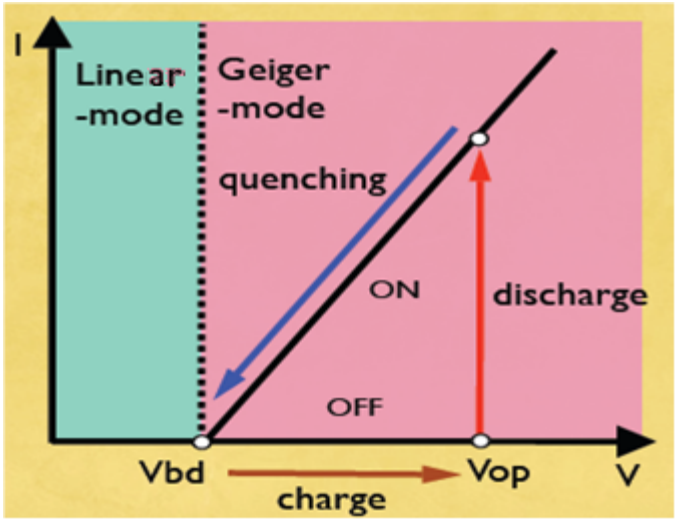

J. Haba, RICH2007

Multi pixel G-APD, called G-APD, MPPC, SiPM, …

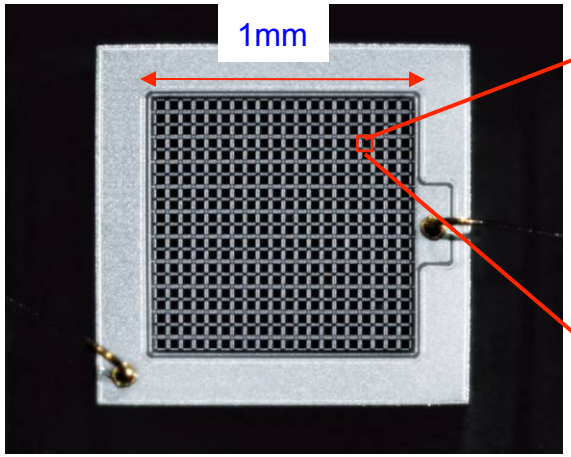

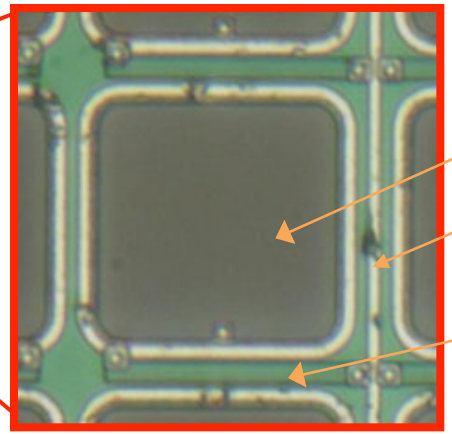

100 – several 1000 pix / mm^2

GM-APD

Bias bus

Quench resistor

Only part of surface is photosensitive!

Sizes up to 6×6 mm^2 now standard.

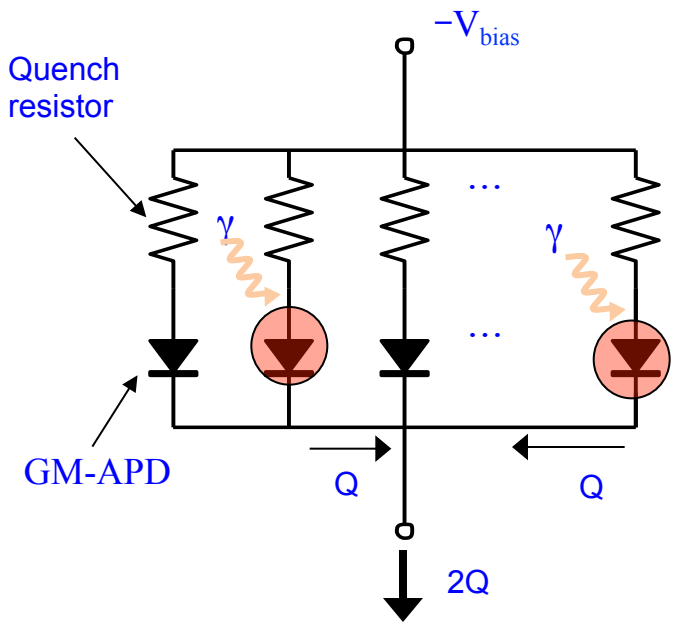

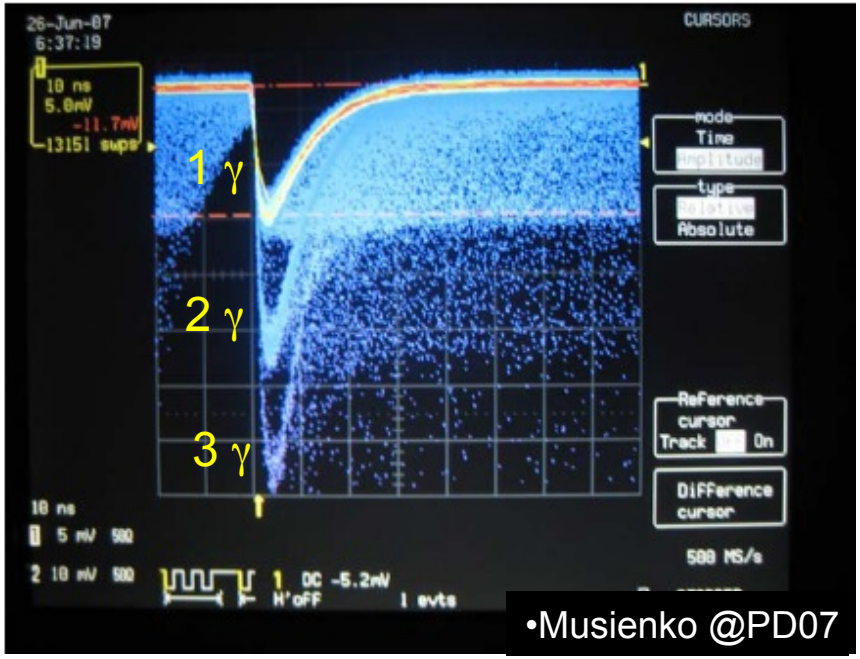

•Musienko @PD07

Quasi-analog detector allows photon counting with a clearly quantized signal

Timing Detector for HL-LHC et al.

NA62 GigaTracker and TDCPix Chips

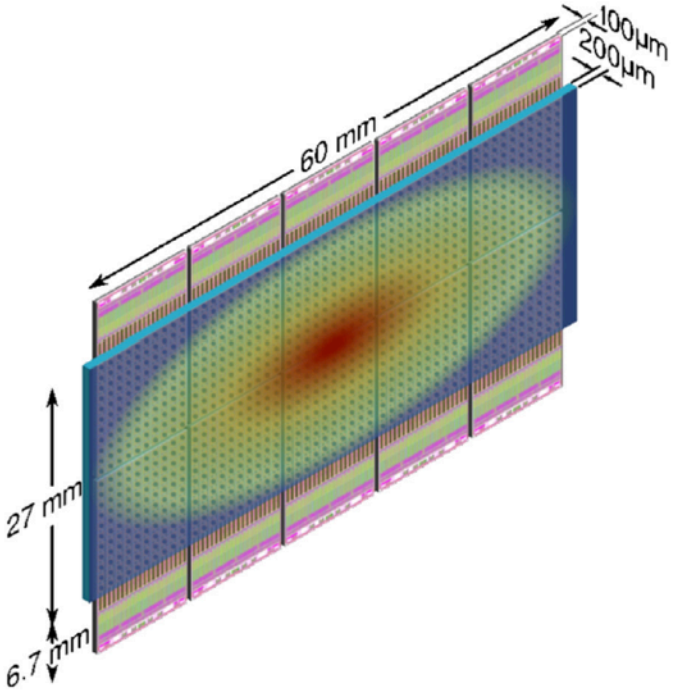

Fig. 2. The TDCPix assembly is composed of a 60.8 mm × 27 mm sensor bump-bonded onto 5 × 2 TDCPix chips. The chip digital and time-to-digital converters logic is located in the 6.7 mm extending outside the sensor.

The NA62 GigaTracker

G. Aglieri Rinella [a], D. Alvarez Feito [a], R. Arcidiacono [e], C. Biino [e], S. Bonacini [a], A. Ceccucci [a], S. Chiozzi [c], E. Cortina Gil [b], A. Cotta Ramusino [c], J. Degrange [a], M. Fiorini [c,d], E. Gamberini [c,d], A. Gianoli [c], J. Kaplon [a], A. Kluge [a], A. Mapelli [a], F. Marchetto [e], E. Minucci [b], M. Morel [a], J. Noël [a], M. Noy [a], L. Perktold [a], M. Perrin-Terrin [a,*], P. Petagna [a], F. Petrucci [c,d], K. Poltorak [a], G. Romagnoli [a], G. Ruggiero [a], B. Velghe [b], H. Wahl [d]

[a] CERN, Switzerland
[b] UCL Louvain, Belgium
[c] INFN Sezione di Ferrara, Italy
[d] Università di Ferrara, Italy
[e] INFN sezione di Torino, Italy

ARTICLE INFO

Article history:
Received 24 March 2016
Received in revised form
9 June 2016
Accepted 10 June 2016

Keywords:
Silicon detector
Ultra fast
NA62
GigaTracker
GTK

MSC:
00-01
99-00

ABSTRACT

The GigaTracker is a hybrid silicon pixel detector built for the NA62 experiment aiming at measuring the branching fraction of the ultra-rare kaon decay $K^+ \to \pi^+\nu\bar{\nu}$ at the CERN SPS. The detector has to track particles in a beam with a flux reaching 1.3 MHz/mm^2 and provide single-hit timing with 200 ps RMS resolution for a total material budget of less than 0.5% X_0 per station. The tracker comprises three 60.8 mm × 27 mm stations installed in vacuum (~10^{-6} mbar) and cooled with liquid C_6F_{14} circulating through micro-channels etched inside a few hundred micron thick silicon plates. Each station is composed of a 200 μm thick silicon sensor read out by 2 × 5 custom 100 μm thick ASICs, called TDCPix. Each chip contains 40 × 45 asynchronous pixels, 300 μm × 300 μm each and is instrumented with 100 ps bin time-to-digital converters. In order to cope with the high rate, the TDCPix is equipped with four 3.2 Gb/s serialisers sending out the data. We will describe the detector and the results from the 2014 and 2015 NA62 runs.

© 2016 Published by Elsevier B.V.

200um silicon sensor with 300umx300um pixels,
100um TDCPix Chip with 100ps time bins
Microchannel Cooling
0.5%X0 per station
0.75GHz of particles in total
1.5MHz/mm^2 in the center.

NA62 GigaTracker and TDCPix Chips

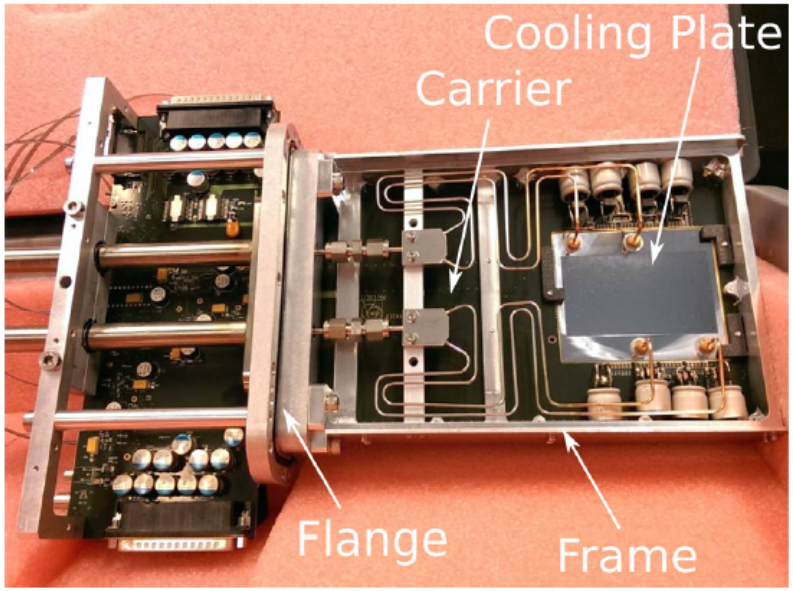

Fig. 4. Picture of the backside (or cooling plate side) of a GigaTracker detector.

The GTK hybrid pixel matrix is made by bump-bonding two rows of five 100 μm thick TDCPix chips to a 200 μ m thick silicon sensor of 60.8 mm × 27 mm as shown in Fig. 2. Both p-in-n and n-in-p sensors can be used. The pixel matrix is organized in 40 columns of 45 pixels each. The pixel size is 300 μm × 300 μm. The chip architecture has been designed to keep the pixel analogue logic separated from the digital logic which is located at the end-of-column region.

Each pixel electrode is connected to a pre-amplifier followed by a discriminator with a tunable threshold. The discriminated signals are then transmitted to the end-of-column where the hit leading time and time-over-threshold (ToT) are measured by time-to-digital-converter (TDC) pairs with 100 ps bins.

Overall the TDCPix chip contains 360 TDC pairs where each TDC pair is shared by five pixels.

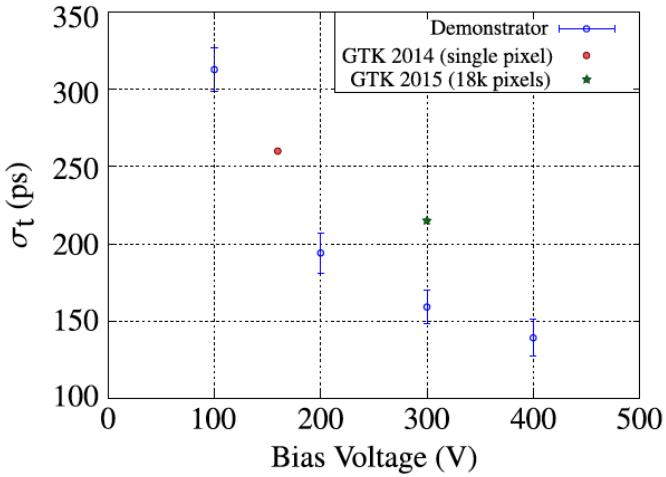

Fig. 7. Hit arrival time resolution as a function of the voltage bias applied to the sensor.

Pileup at HL-LHC, 200 pp collisions per BC

- **Extremely harsh radiation environment in forward detector regions:**
  - Ionizing doses up to 16 kGy for $|\eta| \leq 1.5$ (250 kGy at $\eta = 2.5$)
  - Ch. hadrons up to 7×10^{12} cm^{-2} for $|\eta| \leq 1.5$ (2.3×10^{14} at $\eta = 2.5$)
  - Neutrons up to 1.9×10^{14} cm^{-2} for $|\eta| \leq 1.5$ (1.1×10^{15} at $\eta = 2.5$)

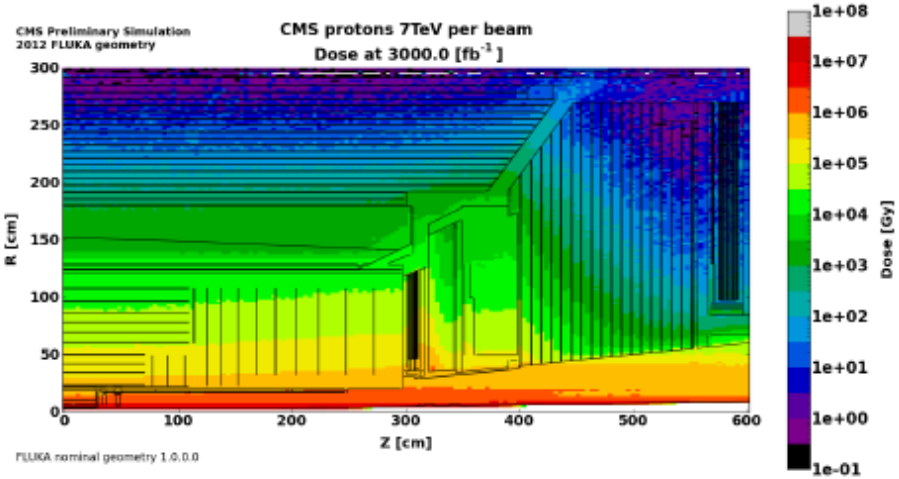

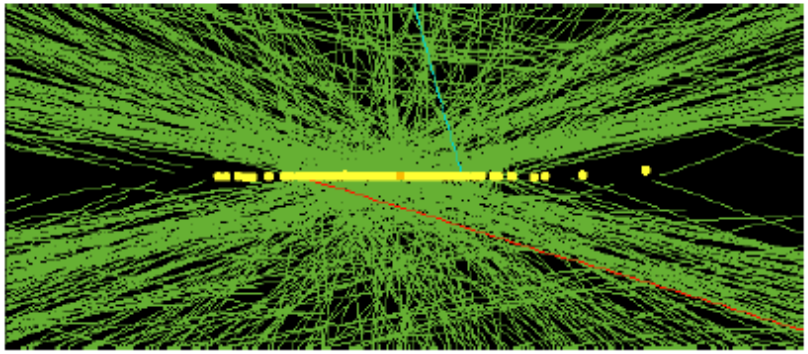

- **Challenging pile-up scenario:**
  - Average pile up $\langle \mu \rangle = 140 - 200$ (compared to current $\langle \mu \rangle \sim 25$)

Potential for a timing layer

By slicing up the bunch crossing region in time intervals of ≤ 30 **ps the level of pile up can be reduced to the current LHC conditions**

CMS Simulation

<μ>	4D Merged Vertex Fraction	3D Merged Vertex Fraction	Ratio of 3D/4D
50	0.5%	3.3%	6.6
200	1.5%	13.4%	8.9

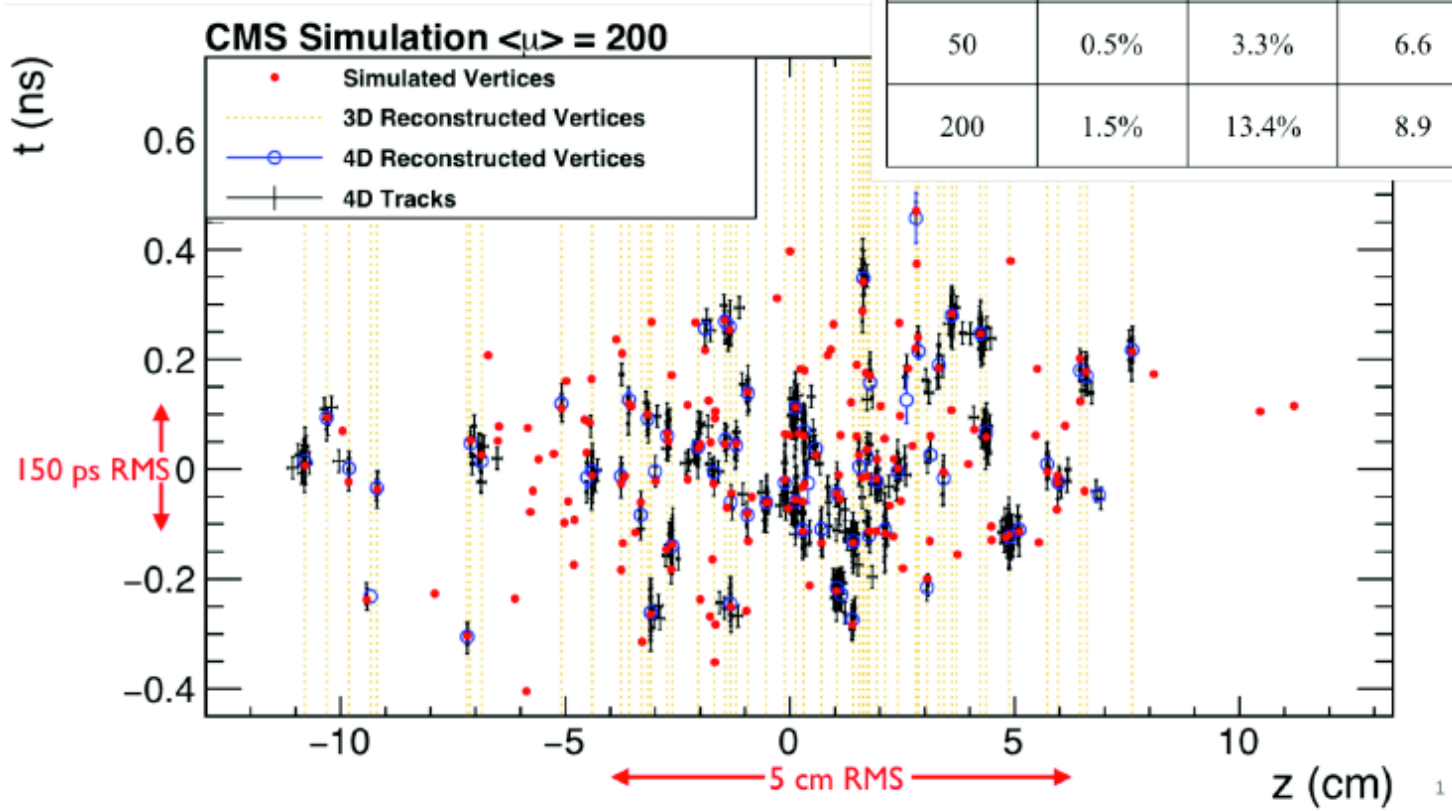

More details in previous J.Bendavid's talk

Overview of technology R&D for precision timing

Outline:

- Optimization of technologies for **single mip timing**
- Recent results and prospects

This is a research field in quick evolution with impressive progress on different technologies from many groups:

- Crystals read-out with Silicon Photo Multipliers (Crystal+SiPM)
- Micro Pattern Gaseous Detectors (MPGD)
- Micro Channel Plates (MCP-PMT)
- Deep Depleted Avalanche Diodes (DDAD)
- Low Gain Avalanche Diodes (LGAD)

Crystal+SiPM MPGD MCP-PMT DDAD LGAD

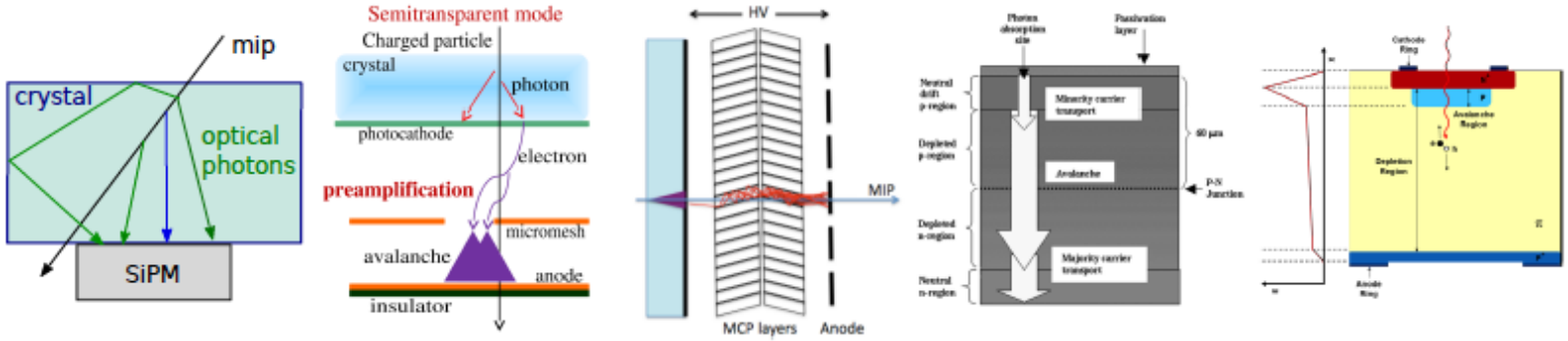

Results from test beam with LSO:Ce

- Test beam study with 150 GeV muons to evaluate timing performance of different crystals and SiPM options*
- Best results with **5 mm thick** LSO:Ce,Ca + NUV-HD FBK SiPMs
- **R&D on SiPMs has large potential for improvement of timing**

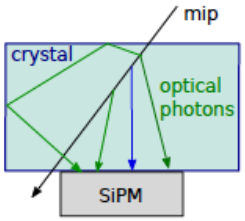

$\sigma_t^{single} = 19.4$ **ps**

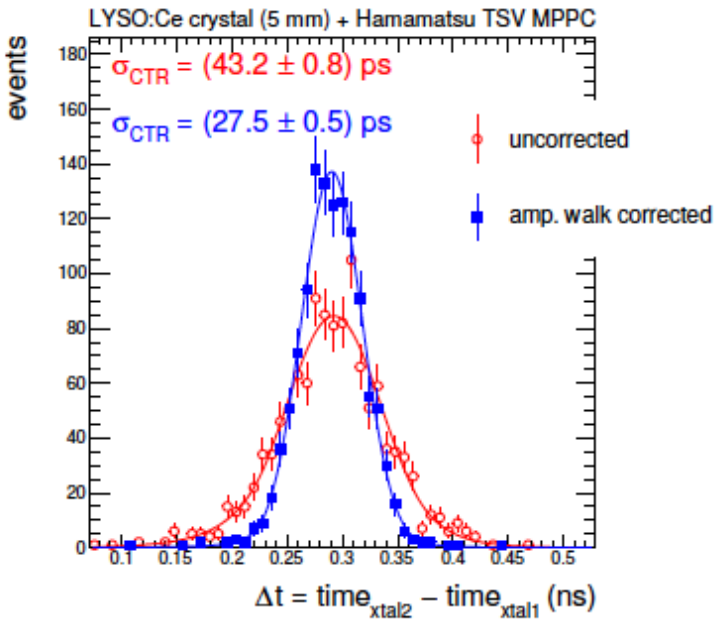

$\sigma_t^{single} = 10.3$ **ps**

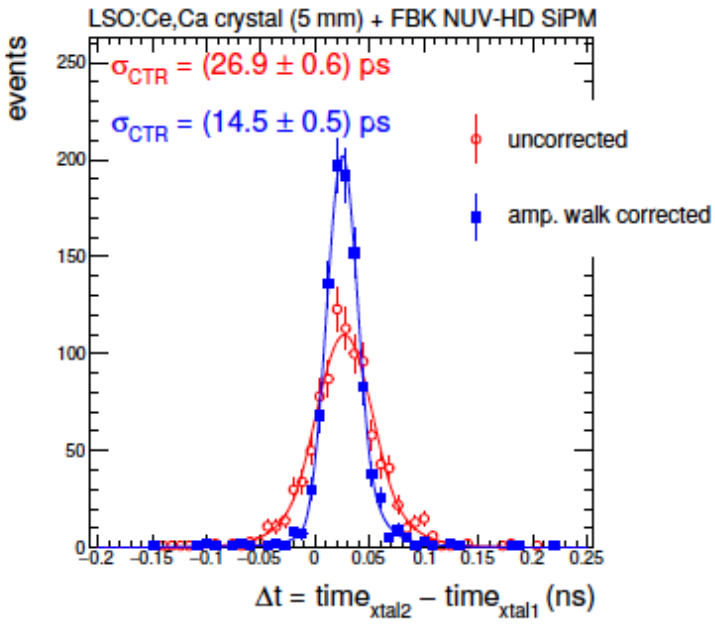

A.Benaglia et al., NIM A 830 (2016) 30-35

In the framework of Crystal Clear Collaboration and TICAL and FAST projects

MCP-PMT: principles of operation

Standard PMT-MCP configuration:
(optical window and photocathode)

- **Cherenkov photons** produced in the front window (or in cherenkov radiator) create primary electrons in the photocathode
- Electrons avalanche amplification within micro-channels with very low time jitter
- High efficiency to mip
- Excellent time resolution

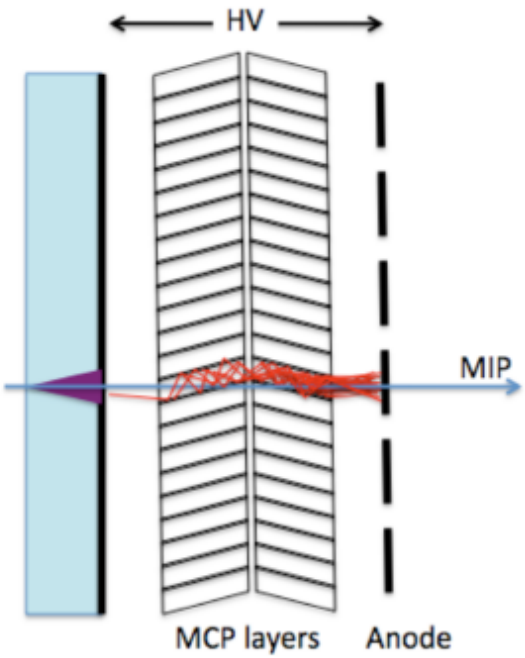

MCP-PMT: best test beam results

Time resolution at the level of $\sigma_t \sim 6 - 10$ ps for mip with single device were achieved by Nagoya (2006) and confirmed by Fermilab tests (A.Ronzhin et al.)*

MCP Time of Flight setup:

- A pair of MCP-PMT (Photek 240)
  - 6 microns MCP hole sizes
  - 40 mm diameter sensitive area
  - MCP gain $\sim 10^6$
- Fused silica window, 9 mm thick
- $\sim$ 80 phe per charged particle

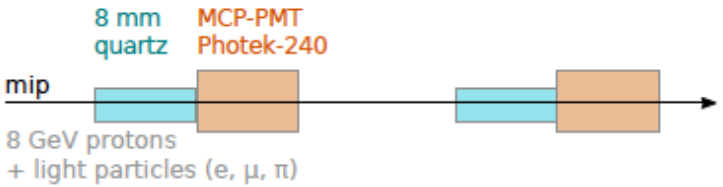

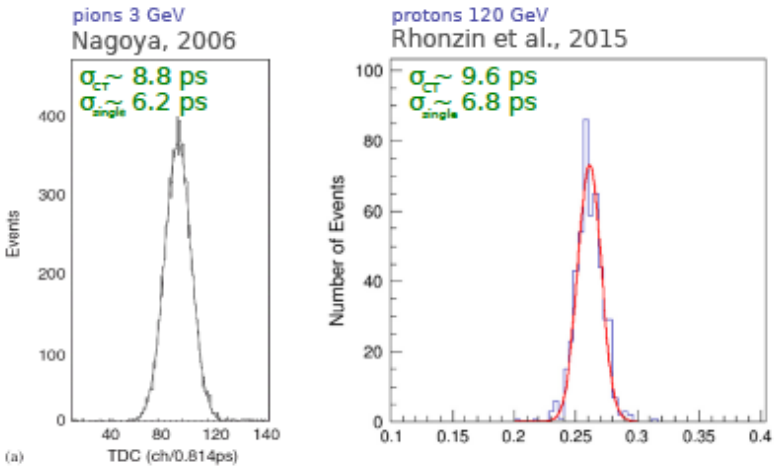

* *K. Inami et al., NIM A 560 (2006) 303-308*
A.Ronzhin et al., NIM A 795 (2015) 288-292

TOF applications

- excellent timing properties require fast light source → Cherenkov radiator directly attached to the MCP-PMT

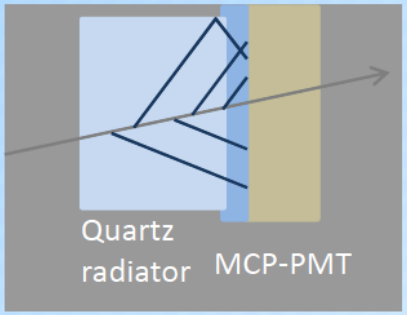

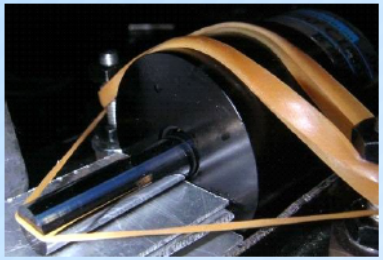

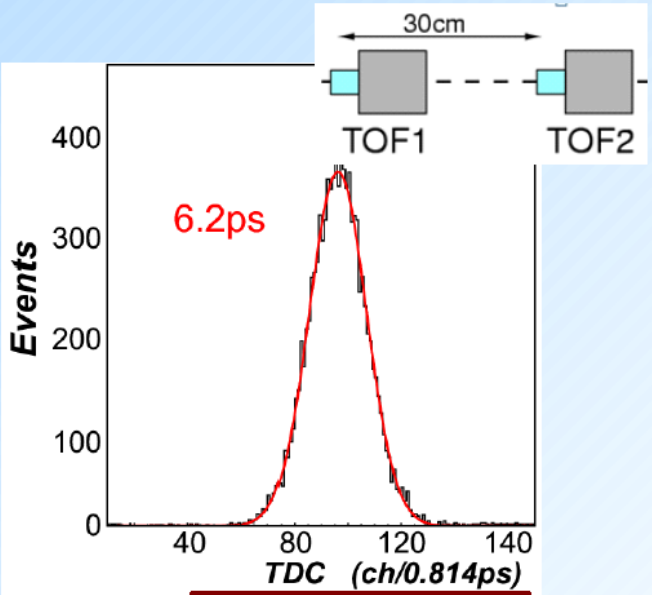

K. Inami @ PD07

- can be used as part of the proximity focusing RICH

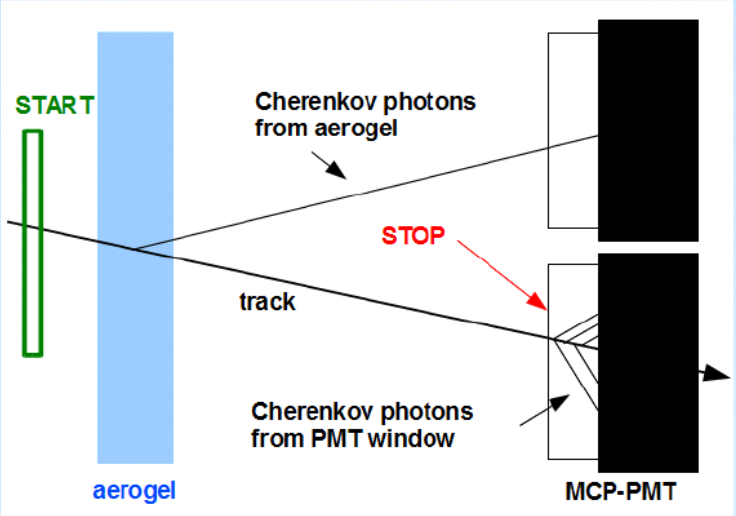

S. Korpar et al. NIM-A572(2007)432

Proximity focusing aerogel RICH with TOF capability

Separation of 2 GeV pions and protons with 0.6 m flight length (start counter s ~ 15 ps).

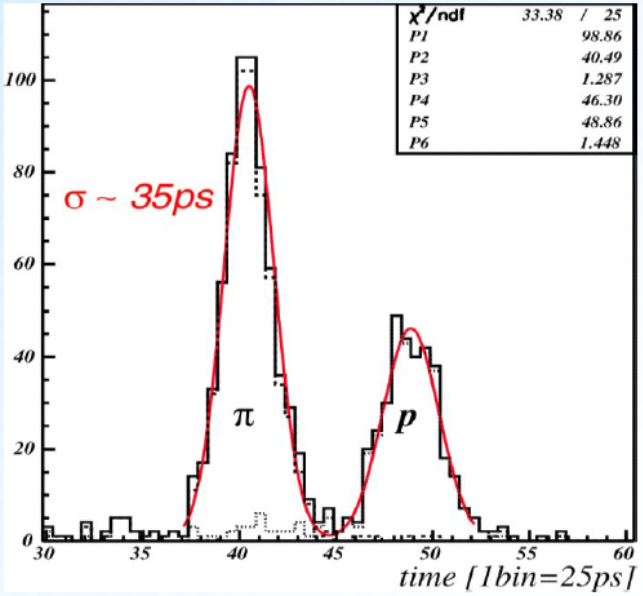

LGAD - Ultra-Fast Silicon Detector

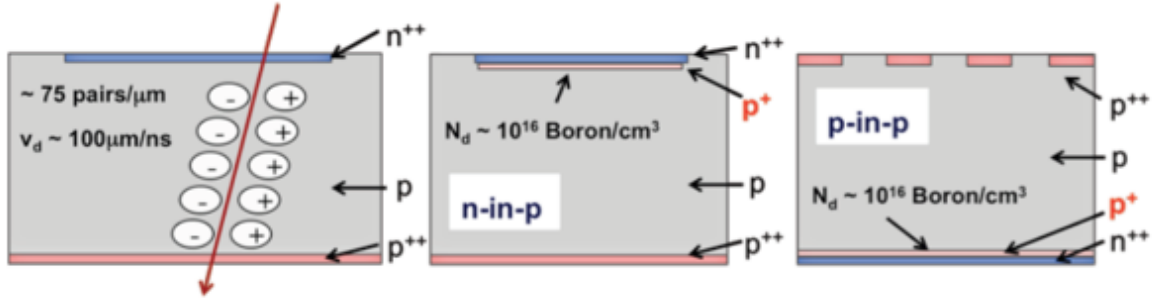

Traditional Silicon Detector **Ultra-Fast Silicon Detector**

Adding a highly doped, thin layer of of p-implant near the p-n junction creates a high electric field that accelerates the electrons enough to start multiplication. Same principle of APD, but with much lower gain.

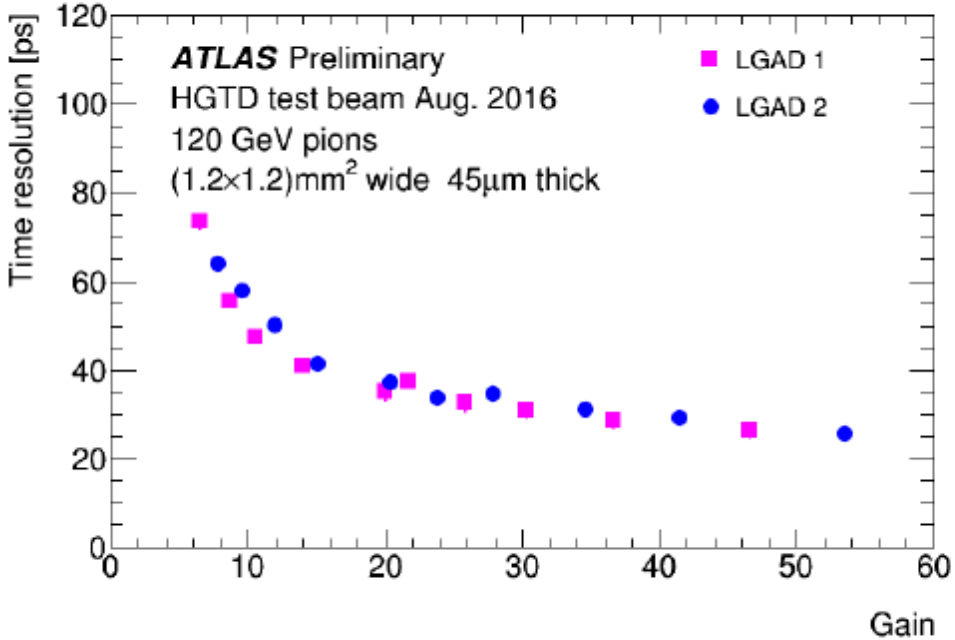

Conclusion

Many novel sensors are finding their way into HEP experiments.

Silicon sensors are being continuously improved with respect to radiation hardness, material budget, position and time resolution. Monolithic Silicon sensors will provide (are providing) a quantum jump in performance/cost …

Progress in microelectronics, low power ADCs, high bandwith data transmission etc. allow a large fraction of the 'trigger' to move to computing farms.

All types of photon sensors are still being used and permanently improved. SiPMs made significant progress and are being applied on a large scale.